

NATIONAL ADVISORY COMMITTEE FOR AERONAUTICS

WARTIME REPORT

ORIGINALLY ISSUED
May 1943 as
Advance Restricted Report 3E22

JET-BOUNDARY CORRECTIONS FOR
REFLECTION-PLANE MODELS IN RECTANGULAR WIND TUNNELS

By Robert S. Swanson and Thomas A. Toll

Langley Memorial Aeronautical Laboratory
Langley Field, Va.

NACA

WASHINGTON

NACA WARTIME REPORTS are reprints of papers originally issued to provide rapid distribution of advance research results to an authorized group requiring them for the war effort. They were previously held under a security status but are now unclassified. Some of these reports were not technically edited. All have been reproduced without change in order to expedite general distribution.



3 1176 01439 3707

NATIONAL ADVISORY COMMITTEE FOR AERONAUTICS

ADVANCE RESTRICTED REPORT.

JET-BOUNDARY CORRECTIONS FOR REFLECTION-PLANE

MODELS IN RECTANGULAR WIND TUNNELS

By Robert S. Swanson and Thomas A. Toll

SUMMARY

A detailed method for determining the jet-boundary corrections for reflection-plane models in rectangular wind tunnels is presented. The method includes the determination of the tunnel span load distribution and the derivation of equations for the corrections to the angle of attack, the lift and drag coefficients, and the pitching-, rolling-, yawing-, and hinge-moment coefficients. The principal effects of aerodynamic induction and of the boundary-induced curvature of the streamlines have been considered. An example is included to illustrate the method. Numerical values of the more important corrections for reflection-plane models in 7- by 10-foot closed wind tunnels are presented.

INTRODUCTION

The influence of the jet boundaries upon the air flow at and behind two-dimensional-flow models and complete models has been rather extensively investigated from theoretical considerations. The results of several of these investigations are given in references 1 to 4. A few experimental checks of the theory have been successfully made. The theoretical methods may be extended to determine the influence of the jet boundaries upon the characteristics of semi-span models mounted on reflection planes in rectangular wind tunnels. One of the walls of a closed wind tunnel may serve as the reflection plane, as shown in figure 1. The jet-boundary corrections are usually larger and the changes in the span load distribution are somewhat greater for reflection-plane models than for complete models, especially with regard to the characteristics of the lateral-control devices. Greater care is therefore required in the computations and more factors

must be considered for reflection-plane-model corrections than for the usual complete-model corrections.

The present investigation was undertaken to develop general methods of calculating the various corrections and methods of determining the changes in the span load distribution caused by the jet boundaries. Numerical values of the more important corrections were calculated for a series of representative models mounted in 7- by 10-foot closed rectangular wind tunnels. The numerical values are presented in the form of graphs and empirical equations in a separate section of the report, in order that the values may be obtained without referring to the detailed calculation procedure. Tables of the numerical values of the jet-boundary-induced upwash velocity for 7- by 10-foot closed wind tunnels are included and should be used if it is desired to compute the corrections for models having unusual proportions. The complete calculation procedure is illustrated in detail by an example.

The basic method used to determine the jet-boundary corrections is to determine the increments of aerodynamic forces and moments acting on a model which is twisted by the amount of the boundary-induced upwash angle. Methods of calculating the boundary-induced upwash angle along the model span and chord and methods of calculating the various jet-boundary corrections, accounting for the principal effects of aerodynamic induction, are presented in separate sections in the present report.

The formulas and corrections presented apply to complete models for which the spans are twice the spans of the reflection-plane models. If a model of only the outer wing panel is tested, the measured characteristics will be for a model of the aspect ratio, taper ratio, and lateral-control-device span ratio actually tested. Additional plan-form corrections - that is, the usual aspect-ratio and taper-ratio corrections plus corrections for the ratio of the lateral-control-device span to the wing span, reference 5 - must therefore be made to determine free-air data for the actual airplane from the corrected data for the model.

SYMBOLS

Γ	circulation strength of vortex
C_L	measured lift coefficient
ΔC_L	increment of lift coefficient
$\Delta C_{L_{s.c.}}$	correction to lift coefficient due to streamline curvature
c_l	section lift coefficient
c_n	section normal-force coefficient
c_h	section hinge-moment coefficient
ΔL_s	increment of lift at any section
C_l	measured rolling-moment coefficient
C_{l_c}	corrected rolling-moment coefficient
ΔC_l	increment of rolling-moment-coefficient correction due to jet boundaries other than reflection plane, based on a reflection-plane rolling-moment coefficient of $1 + \frac{2\Delta C_{l_r}}{C_{l_c}}$
C_{l_δ}/k	rolling derivative due to deflection of lateral-control device (reference 5)
ΔC_{l_r}	half of increment of rolling-moment-coefficient correction due to reflection plane based on unit free-air rolling-moment coefficient
J	aerodynamic-induction factor used in determining ΔC_l
α	angle of attack
$\Delta\alpha$	correction to angle of attack
ΔD_{1s}	increment of induced drag at any section
ΔC_{D_i}	correction to induced-drag coefficient
ΔC_{n_1}	correction to induced-yawing-moment coefficient $\left[(\Delta C_{n_1})_1 + (\Delta C_{n_1})_2 + (\Delta C_{n_1})_3 + (\Delta C_{n_1})_4 + (\Delta C_{n_1})_5 \right]$

4

- $(\Delta C_{n1})_1$ increment of yawing-moment-coefficient correction due to reflection plane
- $(\Delta C_{n1})_2$ increment of yawing-moment-coefficient correction due to boundary-induced aileron upwash and wing loading
- $(\Delta C_{n1})_3$ increment of yawing-moment-coefficient correction due to boundary-induced wing upwash and tunnel aileron loading
- $(\Delta C_{n1})_4$ increment of yawing-moment-coefficient correction due to boundary-induced aileron upwash and flap loading
- $(\Delta C_{n1})_5$ increment of yawing-moment-coefficient correction due to boundary-induced flap upwash and tunnel aileron loading
- $\Delta C_{m_s.c.}$ correction to pitching-moment coefficient due to streamline curvature
- ΔC_h correction to hinge-moment coefficient
- Δc_h correction to hinge-moment coefficient at any section
- ΔH_s increment of hinge-moment correction at any section
- ρ air density
- V free-stream velocity, parallel to X axis
- q dynamic pressure $\left(\frac{1}{2}\rho V^2\right)$
- w induced vertical velocity, parallel to Z axis
- x distance parallel to X axis
- z distance parallel to Z axis
- y distance parallel to Y axis
- \bar{y} centroid of spanwise load
- y_1 spanwise position of trailing vortices
- d effective height of wing above tunnel center line

- b total wing span (twice span of reflection-plane model)
- b_a span of aileron on semispan model
- b_f span of flap on semispan model
- S total wing area (twice area of reflection-plane model)
- S_a area of aileron on semispan model
- S_f area of flap on semispan model
- A aspect ratio $\left(\frac{b^2}{S}\right)$
- λ taper ratio, fictitious chord at tip divided by chord at root
- c chord at any section
- \bar{c} mean chord
- c_B chord at plane of symmetry
- r radius of curvature of streamlines
- h tunnel height
- a tunnel breadth
- a_0 slope per radian of section lift curve
- a_1 slope per radian of lift curve of finite-span wing
- P_{max} maximum ordinate of jet-boundary-induced elliptical load
- F hinge-moment correction factor for jet-boundary-induced elliptical load

Subscripts:

- w wing
- f flap
- a aileron

6

b overhang balance
av average
t tunnel
total total
c corrected
r reflection
p.p. principal part
s.p. supplementary part
 C_m for pitching moments
e effective
s.c. streamline curvature
l.l. lifting line
 y_1 spanwise location of trailing vortex

The axes used are defined in figure 1. All loading and boundary-induced upwash-velocity parameters with primes are based on lift or rolling-moment coefficients not equal to unity.

BOUNDARY-INDUCED UPWASH

Theory

General problem.— The general problem to be solved in determining the jet-boundary corrections for a complete model in a wind tunnel is the determination of the total upwash velocity induced by the jet boundaries. The special problem for a semi-span model mounted as a reflection-plane model to simulate a symmetrically loaded complete model is the determination of the total boundary-induced upwash velocity minus the induced upwash velocity due to the reflection of the semi-span model. The problem of determining the boundary-induced upwash velocity due to unsymmetrical loading devices, such as lateral-control devices on reflec-

tion-plane models, is one of determining not only the total boundary-induced upwash velocity, as for complete models, but also an additional correction due to the non-existence of the reflection wing.

Use of images.— The known boundary conditions to be satisfied are zero normal velocity for closed wind tunnels and constant pressure for open wind tunnels. The boundary conditions for a closed rectangular tunnel may be satisfied by a doubly infinite system of images (reference 1). Figure 1 shows the three-dimensional image arrangement that satisfies the boundary conditions for a semispan model mounted in a closed rectangular wind tunnel. The model is mounted on the X-Z plane - or left wall, looking downstream - and located in the X-Y plane. The reflection wing is shown in phantom and lies along the negative Y axis. It may be noted that this image arrangement is the same as that for a complete model of the same semispan in a tunnel of the same height and twice the width. The images of the wing are represented in this figure as simple horseshoe vortices of semispan $|y_1|$. Any actual span load distribution may be constructed to any desired degree of accuracy from a combination of several horseshoe vortices. The three-dimensional image arrangement is necessary only when it is desired to compute the boundary-induced upwash velocity behind the lifting line, the streamline curvature, or the boundary-induced upwash velocity for models with excessive sweepback.

The boundary-induced upwash velocity at the lifting line may be determined from a two-dimensional image arrangement satisfying the boundary conditions at infinity as shown by Prandtl. Figure 2 shows the two-dimensional image arrangement satisfying the boundary conditions for a single counterclockwise trailing vortex and its reflection (clockwise) located at a distance d above the tunnel center line and at distances equal to y_1 and $-y_1$ from the reflection wall. The single trailing vortex and its reflection represent the trailing vortices of a simple horseshoe vortex with semispan equal to $|y_1|$.

Calculation Methods

Preliminary calculations.— The calculations of general curves of boundary-induced upwash velocity for various image arrangements (figs. 1 and 2) of simple horseshoe or trailing vortices will considerably simplify the labor

involved in determining the boundary-induced upwash velocity for any given model. The boundary-induced upwash velocity behind the lifting line for two values of vortex semispan (image arrangements of fig. 1) was calculated by the methods described in reference 2. The results of the calculations are presented in figure 3 and table I. These calculations apply either to a reflection-plane model in a 7- by 10-foot closed wind tunnel or to a complete (symmetrically loaded) model in a 7- by 20-foot closed wind tunnel.

The boundary-induced upwash velocities at the lifting line were obtained by computing the combined effect of enough of the images, corresponding to the arrangement of figure 2, to give values accurate to the fourth decimal place. The results are given in figure 4 and table II. These values apply to complete models mounted in 7- by 20-foot closed wind tunnels, as well as to reflection-plane models mounted in 7- by 10-foot closed wind tunnels.

The method used to determine the boundary-induced upwash velocity at the lifting line for any given image arrangement is to break up that image arrangement into certain groups, usually vertical rows of images, for which simple summation formulas are available. The sum of the effects of each of these groups may then be determined. The summation formulas for vertical rows of vortices extending from the Y-Z plane to infinity in one direction were developed in references 3 and 4.

Upwash velocity for nonuniform span loading. - Upwash velocity for any nonuniform span loading may be approximated to any desired degree of accuracy by breaking down the actual loading into several steps over each of which the loading is assumed uniform. The boundary-induced upwash velocity may then be determined as the sum of all the components of upwash velocity due to all the stepwise increments. Numerical values for the upwash velocity may be taken directly from the tables rather than from the figures, provided that increments are taken at $\frac{1}{2}$ -foot values of y_1 . If the tunnel walls appreciably alter the span load distribution, as they usually do for a model with a lateral-control device having a relatively large span, the actual tunnel span load distribution should be used instead of the theoretical free-air span load distribution. Methods of approximating the tunnel span load distribution will be presented later in this report. A three- or four-step approximation to the tunnel span-load curve is usually necessary for asymmetrical load conditions. Calculations indicate that very large errors

are introduced by using single uniform loadings for the asymmetrical conditions. For symmetrical load conditions, however, a single-step approximation is usually satisfactory if the span over which the uniform load is assumed to act (called effective span) is properly chosen.

The span-load parameter that will be used in the computations is cc_1A/bC_L , which is equivalent to $2\Gamma A/bVC_L$ (and to L_a as used in reference 6). The upwash angle in radians for unit lift coefficient is w/VC_L for small angles. The formula for determining the local upwash angle is then

$$\frac{w}{VC_L} = \frac{b}{2A} \sum \left(\frac{w}{\Gamma} \right)_{y_1} \Delta \left(\frac{2\Gamma A}{bVC_L} \right)_{y_1} = \frac{b}{2A} \sum \left(\frac{w}{\Gamma} \right)_{y_1} \Delta \left(\frac{cc_1A}{bC_L} \right)_{y_1} \quad (1)$$

where $\left(\frac{w}{\Gamma} \right)_{y_1}$ is obtained from figure 4 or table II and

$\Delta(cc_1A/bC_L)_{y_1}$ is proportional to an increment of load extending from the reflection plane to y_1 . In other words, $\Delta(cc_1A/bC_L)_{y_1}$ is proportional to the strength of the trailing vortex assumed to leave the wing at y_1 .

Boundary-induced upwash angles are given in figure 5 for unit lift coefficient for a 7-foot semispan model of aspect ratio 6 and taper ratio 0.5 and for a unit flap lift coefficient for two ratios of flap span to wing span (called flap-span ratio). The actual span loading is represented by a seven-step approximation. It may be seen from figure 5 that, if the proper value of the effective semispan is used, the upwash angle may be determined satisfactorily by the use of a simple uniform load. The effective span is, of course, dependent upon the particular model-tunnel configuration. Computations for several representative reflection-plane models in 7- by 10-foot closed wind tunnels indicate that good accuracy in the determination of the boundary-induced upwash angle is obtained with the following ratios of effective span to actual span, b_o/b or b_{fe}/b , provided the model semispan is between 6 and 8 feet (the usual values):

Wing:

Rectangular	0.93
Taper ratio, about 0.5	0.88
Taper ratio, about 0.25	0.83
Partial-span flap:	
b_f/b greater than 0.6	1.00
b_f/b less than 0.5	1.30

The span-load parameter that will be used in the computations for the asymmetrical loading condition is $cc_l A/bC_{l_c}$ (or $2\Gamma A/bVC_l$). The upwash angle, however, is most conveniently expressed in terms of a parameter that represents the reflection-plane loading for a rolling-moment coefficient greater than unity, as follows:

$$\left[\frac{w}{V(C_{l_c} + 2\Delta C_{l_r})} \right]' = \frac{b}{2A} \sum \left(\frac{w}{\Gamma} \right)_{y_1} \Delta \left[\frac{cc_l A}{b(C_{l_c} + 2\Delta C_{l_r})} \right]' \quad (2)$$

The primes indicate that the expressions are not true parameters, because the values are not for unit rolling-moment coefficient but for a rolling-moment coefficient equal to $1 + \frac{2\Delta C_{l_r}}{C_{l_c}}$.

CORRECTIONS

General

The jet-boundary corrections may be divided into two groups. The first group consists of all corrections to be applied to a symmetrically loaded model; that is, all forces, moments, and air-flow conditions acting on the reflection-plane model are reflected identically with respect to reflection plane and thus the measured model characteristics are for a symmetrical model. The measured lift, drag, and pitching moment of the model are thus exactly one-half those for a complete model mounted in a wind tunnel of the same height and twice the breadth as the original tunnel, and the boundary-induced upwash velocity is the same as for the complete model in the larger tunnel. The second group of corrections are for the asymmetrical loading condition, such as the loading due to the deflection of a lateral-control device. The loading due to the lateral-control device is reflected into the reflection plane just as it was for the symmetrical case;

but the reflection is undesirable in this case and must be corrected for, as it would not be present on a complete model. Also, the absence of the other wing (the reflection wing) causes the measured rolling and yawing moments to be too large, because the load due to aerodynamic induction existing on the other wing of a complete model will be absent from the measured values of a reflection-plane model.

The corrections will be determined with the proper sign in order that they may be added to the measured values for a closed-throat wind tunnel.

Symmetrical Loading Conditions

Span load distribution.— The correction to the span load distribution need not be determined unless stalling tests or actual span-load-distribution tests are made. Calculations for a few reflection-plane models of usual size in 7- by 10-foot closed wind tunnels indicate that the wing span load distribution is altered by the tunnel walls by an amount equivalent to a change in taper ratio of about 0.05; that is, if the geometrical taper ratio of the model is 0.50, the wing span load distribution in the tunnel corresponds to a wing having a taper ratio of about 0.45. The changes in flap span loading are somewhat greater than the changes in wing span loading. The usual effect of the tunnel walls on the flap span loading is to increase the relative loading over the unflapped portion of the wing and to reduce the relative loading over the flapped portion of the wing. It should be remembered, however, that the type of change in span load distribution caused by the jet boundaries is entirely dependent upon the model-tunnel configuration and that other model-tunnel arrangements might produce effects opposite to those just indicated for a reflection-plane model in a 7- by 10-foot closed wind tunnel.

The span load distribution of the wing in free air must be determined to evaluate the change in loading due to the tunnel walls. The free-air span loading for symmetrical load conditions may easily be obtained from the tables of references 6 and 7 for several different wing-flap combinations. For other flap arrangements or any initial wing twist, the influence lines of reference 5 may be used to estimate the shape of the load curves. The actual load curve may be determined from the condition that

13

the area under the curve of cc_1A/bC_L plotted against $\frac{y}{b/2}$ is equal to unity or, if plotted against y , is numerically equal to $b/2$; that is, the average ordinate is equal to unity.

The increment of boundary-induced load corresponding to a tunnel lift coefficient of unity is obtained by assuming that the wing is twisted an amount equal to the boundary-induced upwash angle w/VC_L . The boundary-induced load is calculated from the influence lines of reference 5. The influence lines give the load at a particular spanwise station for unit changes in angle of attack extending various distances inward from the wing tip. Values of c_sA/b for the wings of reference 5 are given in figure 6 in order that the load parameter $cc_1/c_s\alpha$ used in reference 5 may be converted to $cc_1A/b\alpha$.

The increment of boundary-induced load determined in this fashion may be added to the free-air span-load curve to obtain a first approximation to the tunnel-load curve corresponding to a tunnel lift coefficient of $1 + \frac{\Delta C_L}{C_L}$, where $\Delta C_L/C_L$ is equal to the average ordinate of this increment of boundary-induced load. Because the tunnel lift coefficient $1 + \frac{\Delta C_L}{C_L}$ is greater than unity, a second approximation to the increment of boundary-induced load based on a lift coefficient of $1 + \frac{\Delta C_L}{C_L}$ and the new load distribution must be determined and then a third approximation must be made, and so forth. In order to avoid the necessity for using successive approximations in this fashion, it may be assumed that the values of w/VC_L used for the first approximation need only be multiplied by constants determined from the increase in lift coefficient for each of the remaining approximations; that is, it may be assumed that the change in the shape of the span-load curve would not change the shape of the w/VC_L curves. It was shown that the values of the w/VC_L curve may be computed with satisfactory accuracy when a uniform loading over an effective span is assumed and, inasmuch as the shape of the tunnel-load curve does not change appreciably, this assumption of unchanged w/VC_L curves is reasonable. The increment of boundary-induced load corresponding to the

n^{th} approximation based on a free-air unit lift coefficient (if the shape of the $w/\sqrt{C_L}$ curve is unchanged) is simply equal to the values for the first approximation times $\frac{1}{1 - \frac{\Delta C_L}{C_L}}$. In order to obtain the loading in the tunnel

corresponding to a lift coefficient of $1 + \frac{\frac{\Delta C_L}{C_L}}{1 - \frac{\Delta C_L}{C_L}}$

add to the free-air load this n^{th} approximation. Divide all these values by $1 + \frac{\frac{\Delta C_L}{C_L}}{1 - \frac{\Delta C_L}{C_L}}$ to obtain the tunnel-load curve for unit lift coefficient.

This method of estimating the tunnel span load distribution takes into account the main effects of aerodynamic induction. The method is not exact because the jet-boundary-induced upwash angle $w/\sqrt{C_L}$ is calculated approximately. If desired, the upwash angle corresponding to the tunnel-load curve previously determined can be obtained with great accuracy by using many steps in the stepwise distribution to represent the tunnel-load curve. The calculations can then be repeated with the new values of boundary-induced upwash angle. The process could be repeated until the exact tunnel loading, insofar as lifting-line theory applies, is obtained. It seems, however, that the process is so rapidly convergent that the span loading calculated from the approximate upwash angles is usually satisfactory.

As a check on the convergence, the tunnel span load distribution for a large-span elliptical wing in a circular wind tunnel was computed by the method previously described and the result was compared in figure 7 with the more exact calculation of the tunnel span load distribution made by Millikan (reference 8). It may be noted from figure 7 that the effect of the tunnel walls is opposite in this case to the effect already described for models of usual size in 7- by 20-foot closed wind tunnels or reflection-plane models in 7- by 10-foot closed wind tunnels. Influence lines, similar to those given in reference 5, were determined for an elliptical wing for use in calculating the boundary-induced load increment.

A comparison of the final tunnel-load curve with the original (free-air) load curve indicates the change in span loading caused by the tunnel walls. The increment of load due to streamline curvature may also be added to the original load curve. Because the original curve was obtained, however, from the lifting-line theory rather than from the lifting-surface theory, such an additional step would seem an undue refinement.

Chordwise load distribution.— The chordwise load and the chordwise load distribution at each section are altered by the jet boundaries. The main portion of this change in load is corrected for by the usual induced angle-of-attack correction for the upwash angle at the lifting line. The curvature of the streamlines caused by the jet boundaries effectively changes the airfoil camber, which results in a further change in the chordwise load (and the chordwise load distribution). The corrections due to the change in effective camber may be applied partly as an increased angle-of-attack correction and partly as a correction to the lift, the pitching moment, and the hinge moment.

The general characteristics of the increment of load due to boundary-induced streamline curvature may be estimated from thin-airfoil theory. The shape of the boundary-induced streamlines is, to a first approximation, circular because the boundary-induced upwash angle varies almost linearly along the chord unless very wide-chord models are used (fig. 3).

The chordwise load for an airfoil with circular camber may be broken into two components. One component corresponds to a loading of the flat-plate type, which is similar to the loading due to an angle-of-attack change (also called additional-type loading). The magnitude of the load is determined from the product of the slope of the lift curve and the boundary-induced increase in the angle of inclination of the tangent at the 0.50c point because, for circular camber, the curve at this point is parallel to the chord line connecting the ends of the mean line. Inasmuch as this component of load is similar to the load resulting from a simple angle-of-attack change, it may be applied as an additional angle-of-attack correction. The other component of load is elliptically shaped and its magnitude is determined by the product of the slope of the lift curve and the angular difference between the zero-lift line and the chord line or the 0.50c-point

tangent line. The zero-lift line, for an airfoil with circular camber, is determined by the angle of inclination of the tangent of the 0.75c point. The lift, the pitching-moment, and the hinge-moment corrections are a result of this elliptical component of load.

The location of the lifting line for a plain airfoil may be assumed to be at the 0.25c point and the boundary-induced upwash angle is computed by assuming that the total lift is concentrated at the lifting line. The location of the lifting line for a flapped wing will lie somewhere behind the 0.25c point, depending upon the flap characteristics. The location of the lifting line determines the magnitude and direction of the flat-plate type of load. The two components (flat-plate-load and elliptical load) are equal and positive if the lifting line is located at the 0.25c point. Each component may be expressed as

$$\Delta c_l = 0.25 \frac{a_0 c}{r} \approx 0.25 a_0 c \theta_L \frac{\partial \left(\frac{V}{\sqrt{C_L}} \right)}{\partial x}$$

where r is the radius of curvature of the streamlines. If the lifting line is at the 0.50c point, the flat-plate component of load is zero. The elliptical component is positive and equal to $0.25 a_0 c/r$, because it is independent of the location of the lifting line. If an extensible flap is used, the magnitude and the distribution of the chordwise load must be calculated as though the chord of the airfoil were increased. Because the results of the tests are usually based on the original chord, the final correction must also be reduced to a coefficient based on the original chord.

No correction will be applied directly to the chordwise load distribution but the angle of attack, the lift, the pitching moment, and the hinge moment will be corrected to account for the altered load distribution.

Angle of attack.— The main portion of the angle-of-attack correction is due to the jet-boundary-induced upwash angle at the lifting line. The problem of finding the angle-of-attack correction is, basically, the determination of the angle of attack that the model would require in free air to have the same lift as in the wind tunnel. The correction angle is, then, the difference between the free-air angle of attack and the tunnel angle of attack. If the tunnel span load distribution is determined, the

16

angle-of-attack correction due to the boundary-induced upwash at the lifting line is given as

$$\Delta\alpha = \frac{\Delta C_L}{C_L} \frac{57.3}{a_1} C_L \quad (3)$$

where $\Delta C_L/C_L$ is the increment of boundary-induced load for a tunnel lift coefficient of unity as determined for the span-load calculations.

If the tunnel span load distribution is not determined, the angle-of-attack correction may be calculated by an alternate method that gives values almost identical with those of the method just described. For the alternate method the boundary-induced upwash angle is weighted according to the wing chord at each section and is then averaged across the span. The formula is

$$\Delta\alpha = \frac{57.3 C_L}{S/2} \int_0^{b/2} \frac{w}{V C_L} c \, dy \quad (4)$$

The increment of additional load caused by streamline curvature is dependent upon the relative distance between the lifting line and the 0.50c point as indicated in the section on chordwise load distribution. In the case of the wing, the lifting line may be assumed to be

located at the 0.25c point; thus $0.50 - \frac{x_{l.l.}}{c} = 0.25$.

Because the lifting line due to deflection of a partial-span flap is usually located very near the 0.50c point, it generally is not necessary to apply a correction to the angle of attack for this case. The general equation for the correction to the angle of attack is

$$\Delta\alpha_{s.c.} = \frac{57.3 C_L}{b} \left(0.50 - \frac{x_{l.l.}}{c}\right) \int_0^{b/2} \frac{\partial \left(\frac{w}{V C_L}\right)}{\partial x} \frac{2A}{b} c^2 \, dy \quad (5)$$

where the quantity $\frac{\partial \left(\frac{w}{V C_L}\right)}{\partial x} \frac{2A}{b}$ is equivalent to

$$\sum \left[\frac{\partial \left(\frac{w}{V} \right)}{\partial x} \right]_{y_1} \Delta \left(\frac{c c_L \Delta}{b C_L} \right)_{y_1}$$

Values of $\left[\frac{\partial \left(\frac{w}{V} \right)}{\partial x} \right]_{y_1}$ may be obtained from table I for

$y_1 = 3$ feet and for $y_1 = 6$ feet. The correction angle determined by equation (5) should be added to the lifting-line correction angle as computed from equation (3) or from equation (4).

Lift.— The measured lift in a closed wind tunnel is greater than it would be in free air even though the complete angle-of-attack correction is applied. The increase in lift is due to the elliptically shaped increment of chordwise load caused by streamline curvature. This elliptically shaped increment is applied as a correction to the lift rather than as a correction to the angle of attack in order to correct the maximum lift coefficient. This increment is determined from the slope of the lift curve and the difference in jet-boundary-induced upwash angle at the 0.50c point and at the 0.75c point. The integral

$$\int_0^{b/2} \frac{\partial \left(\frac{w}{V C_L} \right)}{\partial x} \frac{2A}{b} c^2 dy \text{ calculated for the } \Delta \alpha_{s.c.}$$

correction may also be used for the lift correction

$$\Delta C_{L_{s.c.}} = - \frac{a_1 C_L}{4b} \int_0^{b/2} \frac{\partial \left(\frac{w}{V C_L} \right)}{\partial x} \frac{2A}{b} c^2 dy \quad (6)$$

where a_1 is used instead of a_0 to account approximately for aerodynamic induction.

If the lifting line can be assumed to be located at the 0.25c point, as in the case of the wing, equation (6) may be written for the wing lift correction as

$$\left(\Delta C_{L_{s.c.}} \right)_w = - \left(\Delta \alpha_{s.c.} \right)_w \frac{a_1}{57.3} \quad (7)$$

A small correction to the lateral center of pressure, which is determined from the rolling moment, may be obtained by performing a moment integration of the streamline curvature load, as

$$\Delta C_{l_{s.c.}} = \frac{a_1 C_L}{S b^2} \int_0^{b/2} \frac{\partial \left(\frac{w}{\sqrt{C_L}} \right)}{\partial x} \frac{2A}{b} c^2 y \, dy$$

It should be noted that this increment is based on the complete span b rather than on the model span $b/2$.

Pitching moment.— The pitching-moment coefficient must be corrected for the elliptical component of the boundary-induced load. The correction is

$$\Delta C_m = \frac{C_L a_o x_{C_m}}{4 b \bar{c}_w} \left[\frac{\bar{c}_w}{4 x_{C_m}} \left(1 - \frac{a_1}{a_o} \right) + \frac{a_1}{a_o} \right] \int_0^{b/2} \frac{\partial \left(\frac{w}{\sqrt{C_L}} \right)}{\partial x} \frac{2A}{b} c^2 dy \quad (8)$$

where the factor $\left[\frac{\bar{c}_w}{4 x_{C_m}} \left(1 - \frac{a_1}{a_o} \right) + \frac{a_1}{a_o} \right]$ accounts approximately for the effects of aerodynamic induction and reduces to unity if the moments are taken about a line through $\bar{c}_w/4$. The distance x_{C_m} is measured between the line about which the moments are computed and the midchord at the spanwise centroid of the elliptical load $\bar{y}_{s.c.}$ where

$$\bar{y}_{s.c.} = \frac{\int_0^{b/2} \frac{2A}{b} \frac{\partial \left(\frac{w}{\sqrt{C_L}} \right)}{\partial x} c^2 y \, dy}{\int_0^{b/2} \frac{2A}{b} \frac{\partial \left(\frac{w}{\sqrt{C_L}} \right)}{\partial x} c^2 dy} \quad (9)$$

Downwash behind wing.— The correction to the downwash behind a reflection-plane model is determined from the boundary-induced upwash curves previously computed. The

general methods of reference 2 should be used to determine the downwash-angle correction.

Drag.- The induced-drag correction is determined from the generalized Kutta-Joukowski law. The boundary-induced upwash angle and the tunnel span loading are used in the computation of the induced-drag correction. The upwash angle at each section must be multiplied by the loading at that section and the result integrated mechanically. In order to establish the method and to determine the proportionality constants, the integration formula will be developed.

The increment of induced drag at any section due to the tunnel walls is

$$\Delta D_{1s} = \rho w \Gamma dy \quad (10)$$

and the increment of induced-drag coefficient for the wing is

$$\Delta C_{D1} = \frac{4}{V^2 S} \int_0^{b/2} w \Gamma dy \quad (11)$$

where the product $w\Gamma$ is the sum of all component products of wing and flap upwash velocity and circulation

$$w\Gamma = \frac{bV^2}{2A} \left[\left(\frac{w}{V C_{L_w}} \right) \left(\frac{c c_{lA}}{b C_{L_w}} \right) C_{L_w}^2 + \left(\frac{w}{V C_{L_f}} \right) \left(\frac{c c_{lA}}{b C_{L_f}} \right) C_{L_f}^2 + \left(\frac{w}{V C_{L_w}} \right) \left(\frac{c c_{lA}}{b C_{L_f}} \right) C_{L_w} C_{L_f} + \left(\frac{w}{V C_{L_f}} \right) \left(\frac{c c_{lA}}{b C_{L_w}} \right) C_{L_w} C_{L_f} \right] \quad (12)$$

A correction to the lateral center of pressure of the induced-drag force may be obtained by integrating the increment of drag given in equation (10) for the yawing-moment coefficient

$$\Delta C_{n1} = - \frac{2}{V^2 S b} \int_0^{b/2} w \Gamma y dy \quad (13)$$

Hinge moments.- The measured hinge moments of the

high-lift device and lateral-control device should be corrected for the component of elliptical load caused by the curvature of the streamlines. The hinge-moment correction is determined from an integration of the moment about the hinge axis of this load on the high-lift device or on the control surface. The integration must be performed over the entire surface - both chordwise and spanwise - because, in general, the correction varies along the span. The chordwise integration can be performed analytically because the shape of the load is known to be nearly elliptical. The increment of load at any section is determined from the expression for the area of an ellipse as

$$\Delta L_s = \frac{1}{4} \pi P_{\max} c \quad (14)$$

where P_{\max} is the maximum ordinate of the elliptical load. The increment of load is also equivalent to

$$\Delta L_s = \frac{C_{L\alpha} a_0 q b}{8A} \left[\frac{\partial \left(\frac{w}{\sqrt{C_L}} \right)}{\partial x} \frac{2A}{b} c^2 \right] \quad (15)$$

The increment of hinge moment ΔH_s at any section is obtained by a moment integration about the hinge axis of the part of the elliptical load over the movable surface, as

$$\Delta H_s = \frac{c^3}{4} P_{\max} \int \sqrt{1 - \left(\frac{x}{c/2} \right)^2} \left(\frac{x}{c/2} + \frac{c_f}{c/2} - 1 \right) d \left(\frac{x}{c/2} \right) \quad (16)$$

where $P_{\max} \sqrt{1 - \left(\frac{x}{c/2} \right)^2}$ is the ordinate of the elliptical load. The value of P_{\max} is obtained by solving equations (14) and (15) and is substituted in equation (16) to give

$$\Delta H_s = \frac{C_{L\alpha} a_0 q b}{8\pi A} \left[\frac{\partial \left(\frac{w}{\sqrt{C_L}} \right)}{\partial x} \frac{2A}{b} c^2 \right] c \int \sqrt{1 - \left(\frac{x}{c/2} \right)^2} \left(\frac{x}{c/2} + \frac{c_f}{c/2} - 1 \right) d \left(\frac{x}{c/2} \right)$$

where the integral

$$\int \sqrt{1 - \left(\frac{x}{c/2} \right)^2} \left(\frac{x}{c/2} + \frac{c_f}{c/2} - 1 \right) d \left(\frac{x}{c/2} \right)$$

will be known as the hinge-moment correction factor for elliptical load F and the integration is carried across the flap and across any overhang type of balance. The results of the integration are presented in figure 8 as a function of the ratio of the flap chord to the airfoil chord c_f/c or of the aileron chord to the airfoil chord c_a/c , and of the overhang balance chord ratios c_b/c_f and c_b/c_a . The corrections to the flap hinge-moment coefficient may now be expressed as

$$\Delta C_h = \frac{C_{L\alpha} a_0 b}{8\pi A S_f \bar{c}_f} \int \left[\frac{\partial \left(\frac{\kappa}{\sqrt{C_L}} \right)}{\partial x} \frac{2A}{b} c^3 \right] F dy \quad (17)$$

where the spanwise integration across the flap must be performed mechanically. The correction to the aileron hinge-moment coefficient may be determined by performing the integration over the limits of the aileron span rather than of the flap span, as indicated in equation (17), and by using S_a and c_a . It should be noted that F is a function of only c_f/c (or c_a/c) and c_b/c_f (or c_b/c_a) and will therefore have the same value at all sections of constant-percentage-chord flaps or ailerons. The effect of aerodynamic induction on the hinge-moment correction due to streamline curvature is small and will be neglected.

Asymmetrical Loading Conditions

Span load distribution.— The jet boundaries have a pronounced effect upon the span load distribution of asymmetrical load devices on reflection-plane models. In order to determine the rolling- and yawing-moment corrections, part of the computations to determine the tunnel span load distribution must be made. The actual distribution may be obtained by a small amount of additional work and a more accurate estimate of the rolling-, yawing-, and hinge-moment corrections is then possible.

The tunnel span load distribution is determined by adding to the free-air load the increment of load due to the reflection plane and the increment of load due to the other jet boundaries and by then reducing this total load to that for a rolling-moment coefficient of unity. The influence lines of reference 5 may be used to estimate the free-air load and the reflection-plane load increment. It should be noted that the reflection-plane load increment

is simply the load induced on the reflection wing for an asymmetrical load on the real wing, that is, the load curve for a reflection-plane model in free air (no jet boundaries except the reflection plane) is obtained by adding the free-air load at $-y$ to that at y .

The load parameter $cc_l/c_s\alpha$ of reference 5 should be changed to cc_lA/bC_{l_c} for convenient use in the computation of jet-boundary corrections. The conversion may be made as

$$\frac{cc_lA}{bC_{l_c}} = \frac{cc_l}{c_s\alpha} \frac{c_sA}{b} \frac{C_{l_c}}{\alpha} \quad (18)$$

where values of c_sA/b are given in figure 6 for the wings of reference 5 and values of C_{l_c}/α may be determined from figure 16 of reference 5 - that is, $C_{l_c}/\alpha = 0.5 C_{l_8}/k$. The conversion may be made graphically from the condition that the moment of the area under the curve of cc_lA/bC_{l_c} against $\frac{y}{b/2}$ is equal to 4.0 or, if plotted against y , is numerically equal to $4.0(b/2)^2$ or b^2 .

The increment of load due to the jet boundaries (other than the reflection plane) is obtained from the influence lines of reference 5 by the same general methods used in determining the increment of boundary-induced load for the symmetrical loading condition; that is, the wing is assumed to be twisted by the amount of the boundary-induced upwash angle and the corresponding increment of load is obtained from the influence lines.

The boundary-induced upwash angle should, strictly speaking, be determined by a process of successive approximations because it also depends upon the shape of the tunnel span load curve. It is usually satisfactory, however, to represent the reflection-plane loading by a three- or four-step approximation, and to calculate the corresponding boundary-induced upwash angle by the methods suggested in the section on boundary-induced upwash velocity. The increment of load calculated from this boundary-induced upwash angle will correspond to a rolling-moment

coefficient of $1 + \frac{2\Delta C_{l_r}}{C_{l_c}}$, which is the reflection-plane

rolling-moment coefficient for unit free-air rolling-moment coefficient. (The use of these factors will be made clearer in the section on rolling-moment corrections and in the illustrative example.) The increment of load must therefore be increased to correspond to the rolling-moment coefficient occurring in the tunnel for unit free-air rolling-moment coefficient ($C_{l_c} = 1.0$). It will be shown later in the section on rolling-moment corrections that the tunnel rolling-moment coefficient for unit free-air rolling-moment coefficient is equal to

$$\frac{1 + \frac{2\Delta C_{l_r}}{C_{l_c}}}{1 - \frac{\Delta C_l}{1 + \frac{2\Delta C_{l_r}}{C_{l_c}}}}$$

where ΔC_l is the moment of the increment of boundary-induced load corresponding to the reflection-plane load. This increment must therefore be multiplied by

$$\frac{1}{1 - \frac{\Delta C_l}{1 + \frac{2\Delta C_{l_r}}{C_{l_c}}}}$$

before it is added to the reflection-plane load. The tunnel span load distribution for unit tunnel rolling-moment coefficient is obtained by so reducing the ordinates of this curve that the moment is equal to $4.0 (b/2)^2$ or (the same thing) by multiplying by the rolling-moment-coefficient correction

$$C_{l_c}/C_l = \frac{1 - \frac{\Delta C_l}{1 + \frac{2\Delta C_{l_r}}{C_{l_c}}}}{1 + \frac{2\Delta C_{l_r}}{C_{l_c}}}$$

The tunnel span load distribution, as well as the rolling-moment-coefficient correction, has thus been determined. The explanation of the determination of the rolling-moment correction will be given in the next section in some detail to explain further the method of determining the tunnel loading and to present alternate methods of determining the rolling-moment correction that do not require the determination of the tunnel loading.

Rolling moment.— The correction to the rolling moment will be determined in two parts. The first part of the correction is caused by the absence of the reflection wing and the load increment due to the reflection plane. This part of the correction depends not upon the model-tunnel configuration but only upon the characteristics of the model itself; consequently, it was possible to calculate the correction increment for several wing-aileron combinations from the data of reference 5. The aileron span load distributions were mechanically integrated to determine the moment of the load on the absent wing $\Delta C_{l_r}/C_{l_c}$ in terms of the free-air moment of the total load. Not only because the reflection wing is nonexistent but also because an equal load is induced on the real wing by the reflection image, twice this absent-wing moment must be applied as a correction. The correction is presented in figure 9 in an easily used form, $1 + \frac{2\Delta C_{l_r}}{C_{l_c}}$ as a function of the aileron span ratio — that is, ratio of aileron span to wing semispan — for ailerons extending inward from the wing tips.

The second part of the rolling-moment correction ΔC_{l_r} results from the moment about the plane of symmetry of the boundary-induced load. The method of calculating the boundary-induced load has already been explained in connection with the determination of the tunnel span load distribution. If the tunnel span loading is not determined, this second increment may be calculated from simple strip theory — neglecting aerodynamic induction, that is, the effects of the velocities induced by the trailing-vortex system — and multiplied by a factor $A/(A + J)$ to account approximately for the effects of aerodynamic induction.

The value of J depends upon the distribution of boundary-induced upwash angle and the model taper ratio but is practically independent of aspect ratio and only slightly dependent upon the slope of the section lift

curve. Figure 10 gives some values of J as a function of taper ratio for three distributions of boundary-induced upwash angle. The corresponding upwash-angle distribution is also given in figure 10 and corresponds to various aileron-span ratios for reflection-plane models in 7- by 10-foot closed wind tunnels.

The formula for determining the second increment of the correction is

$$\Delta C_l = \frac{A^2 a_0}{b^3 (A + J)} \int_0^{b/2} \left[\frac{w}{V(C_{l_c} + 2\Delta C_{l_r})} \right]^2 cy dy \quad (19)$$

where $\left[\frac{w}{V(C_{l_c} + 2\Delta C_{l_r})} \right]^2$ is the boundary-induced upwash

angle corresponding to the free-air load plus the reflection-plane load increment. The quantity ΔC_l therefore corresponds to this reflection-plane load and must be divided by

$1 + \frac{2\Delta C_{l_r}}{C_{l_c}}$ in order to be based on unit tunnel rolling-moment coefficient.

The final corrected rolling-moment coefficient C_{l_c} is

$$C_{l_c} = C_l - 2\Delta C_{l_r} - \frac{\Delta C_l}{1 + \frac{2\Delta C_{l_r}}{C_{l_c}}} C_l$$

or

$$C_{l_c} = \frac{C_l \left(1 - \frac{\Delta C_l}{1 + \frac{2\Delta C_{l_r}}{C_{l_c}}} \right)}{1 + \frac{2\Delta C_{l_r}}{C_{l_c}}} \quad (20)$$

where $1 + \frac{2\Delta C_{l_r}}{C_{l_c}}$ is obtained from figure 9 and ΔC_l may

be obtained either from equation (19) or as follows:

$$\Delta C_l = \frac{1}{b^2} \int_0^{b/2} \Delta \left[\frac{cc_l A}{b(C_{l_c} + 2\Delta C_{l_r})} \right]^2 y dy \quad (21)$$

where $\Delta \left[\frac{cc_l A}{b(C_{l_c} + 2\Delta C_{l_r})} \right]^2$ is the increment of boundary-induced load obtained from the span-load calculations for the reflection-plane load $C_{l_c} + 2\Delta C_{l_r}$.

The effect of streamline curvature was not included in equation (20) because calculations for several models showed that the effect was small enough to be neglected.

The rolling-moment coefficients as computed from equation (20) are of the correct magnitude but apply to a wing angle of attack slightly different from the geometric angle of attack corrected for the symmetrical-load boundary-induced upwash angle determined for zero rolling moment. The effective change in wing angle of attack results from the aileron boundary-induced upwash angle and the reflection-plane induced angle. The fact that the corrected rolling-moment coefficients really apply to a slightly different wing angle of attack is of importance only near the stall or for aileron arrangements particularly sensitive to angle-of-attack changes and is usually neglected. The angle change is usually small, less than $\frac{1}{8}^\circ$.

Induced yawing moment.— The correction to the induced yawing moment results from the interaction of the several components of boundary-induced upwash velocity and the several components of load as well as from the reflection image and the absence of the reflection wing. The calculation procedure will be to determine separately each component of the correction and then to sum up the various components as follows:

$$\Delta C_{n_1} = (\Delta C_{n_1})_1 + (\Delta C_{n_1})_2 + (\Delta C_{n_1})_3 + (\Delta C_{n_1})_4 + (\Delta C_{n_1})_5 \quad (22)$$

where the various components are defined in the symbols.

Values of the correction due to the reflection plane $(\Delta C_{n_1})_1$ were calculated from the influence lines of ref-

erence 5 for a series of aileron-span ratios for the plane wing and for flap-span ratios of 0.4 and 0.7. This part of the yawing-moment correction is due solely to the reflection plane and does not depend upon the tunnel-model dimensions. The effect of flap span proved to be negligible; so the values of the correction as presented in figure 11 in the form of curves of $(\Delta C_{n1})_1 / 0_{1c} C_L$ against

aileron-span ratio for ailerons extending inward from the tips are therefore for values of the lift coefficient equal to the measured lift coefficient. The other components are determined from equation (13) where the product $w\Gamma$ is defined by the subscripts a, s, 4, and s. (See SYMBOLS.) All components of boundary-induced upwash velocity and load have already been calculated in the form of parameters that are easily converted to the product $w\Gamma$.

Hinge moments.— The jet-boundary corrections to the hinge moments of lateral-control devices are usually small. The correction due to the elliptical streamline curvature load for the symmetrical loading condition has already been presented. Another small correction exists because the load due to aileron deflection is greater in the wind tunnel than in free air. Although the load due to aileron deflection may be as much as 15 or 20 percent greater in the wind tunnel, the correction to the hinge moments is very small because the greater part of the boundary-induced load is of the additional type (similar to that produced by an angle-of-attack change), which has only a small load over the aileron portion of the wing. The correction is calculated from the average difference between the span loading due to the lateral-control device in the wind tunnel and the loading in free air due to a given aileron deflection. Because the correction is small, the increment of load at the aileron center section

$$\Delta \left[\frac{cc_{1A}}{b(C_{1c} + 2\Delta C_{1r})} \right]^1 + \Delta \left(\frac{cc_{1A}}{b0_{1c} r} \right)$$

will usually be sufficient for the calculation. The correction to the aileron hinge-moment coefficient is then assumed to equal the correction to the section hinge-moment coefficient of the aileron center section (or of some other typical section).

$$\Delta C_h \approx \Delta c_h = - \frac{b0_{1c}}{cA} \frac{\partial c_h}{\partial c_n} \left\{ \Delta \left[\frac{cc_{1A}}{b(C_{1c} + 2\Delta C_{1r})} \right]^1 + \Delta \left(\frac{cc_{1A}}{b0_{1c} r} \right) \right\} \quad (23)$$

where $\partial c_h / \partial c_n$ may be determined experimentally or from section data such as reference 9 for plain-flap lateral-control devices. The hinge-moment correction resulting from the aileron-load streamline curvature is usually small enough to be neglected.

**NUMERICAL VALUES OF CORRECTIONS FOR MODELS IN
 7- BY 10-FOOT CLOSED WIND TUNNELS**

Some numerical values of the more important corrections were computed for various reflection-plane models mounted in 7- by 10-foot closed wind tunnels. Cross plots were made to determine the variation of the corrections with each of the model parameters - Λ and λ , for example - and the results are presented as graphs and empirical equations that may easily be used to estimate the values of the corrections for almost any model. The computations were made by using the load curves and the chord distributions of reference 5 for constant-percentage-chord flaps extending outward from the plane of symmetry and for constant-percentage-chord ailerons extending inward from the wing tip. The values of the corrections presented should be sufficiently accurate for models that deviate slightly from these conditions. The corrections are given in terms of the measured lift and the measured rolling-moment coefficients.

The corrections to the angle of attack, the lift, the drag, and the yawing-moment coefficients for symmetrical loading conditions are presented in figure 12 for wings having $\lambda = 0.5$ and without partial-span flaps. The corresponding corrections for models of any taper ratio and flap-span ratio may be determined by substituting the values obtained from figure 12 in the following empirical equations:

$$\Delta \alpha = \left(\frac{\Delta \alpha}{C_L} \right)_{p.p.} \left[1 - 0.063 (\lambda - 0.5) \right] \left[C_{L_w} + 0.90 C_{L_f} \right]$$

$$\Delta C_{L_{s.c.}} = \left(\frac{\Delta C_{L_{s.c.}}}{C_L} \right)_{p.p.} \left[1 - 0.116 (\lambda - 0.5) \right] \left\{ C_{L_w} + \left[1 + 0.160 \left(1 - \frac{b_f}{b/2} \right) \right] C_{L_f} \right\}$$

$$\Delta C_{D1} = \left(\frac{\Delta C_{D1}}{C_{L^2}} \right)_{p.p.} \left[1 - 0.080 (\lambda - 0.5) \right]$$

$$\left\{ C_{L_w}^2 + 2 \left[1 + 0.20 \left(1 - \frac{b_f}{b/2} \right) \right] C_{L_w} C_{L_f} + \left[1 + 0.65 \left(1 - \frac{b_f}{b/2} \right) \right] C_{L_f}^2 \right\}$$

$$\Delta C_{n1} = \left(\frac{\Delta C_{n1}}{C_{L^2}} \right)_{p.p.} \left[1 + 0.130 (\lambda - 0.5) \right]$$

$$\left\{ C_{L_w}^2 + \left[1 - 0.25 \left(1 - \frac{b_f}{b/2} \right) \right] \left[2C_{L_w} C_{L_f} + C_{L_f}^2 \right] \right\}$$

The corrections to the rolling- and the yawing-moment coefficients for asymmetrical loading conditions may be determined from figure 13. The principal curves of this figure are drawn for models having $\frac{b}{s} = 7$ feet and $\lambda = 0.50$.

Supplementary curves on the same figure give additional correction increments that account for the effect of other spans and other taper ratios. The total corrections are obtained by adding the additional increments to the corrections obtained from the principal curves, as follows:

$$C_{l_c} = \left[\left(\frac{C_{l_c}}{C_l} \right)_{p.p.} + \left(\frac{C_{l_c}}{C_l} \right)_{s.p.} \right] C_l$$

$$\Delta C_{n1} = \left[\left(\frac{\Delta C_{n1}}{C_l C_L} \right)_{p.p.} + \left(\frac{\Delta C_{n1}}{C_l C_L} \right)_{s.p.} \right] C_l C_L$$

The streamline-curvature correction to the hinge-moment coefficients of plain or balanced (overhang type of balance) flaps and ailerons were computed. The balance chord is assumed to be a constant percentage of the flap or aileron chord, and the flaps and ailerons are also of constant-percentage types. Figure 14 gives values of the

parameter $\Delta C_{L A^2} \left(\frac{c_f}{c} \right)^2 / C_L b^2 F$ for various flap- and

aileron-span ratios and various taper ratios. The factor F is taken from figure 8.

It should be remembered that the streamline-curvature correction to the hinge moments is a function of the cube of the chord and comparatively minor variations in plan form, such as tip shape, thus may change the correction by 10 or 15 percent for a given wing span and a given aspect ratio. The value of the correction that is determined for a wing with linear taper in the following illustrative example indicates the possible change in the hinge-moment correction with plan-form details. The correction is usually fairly small, however, so changes of 10 to 15 percent in its magnitude are not too critical.

The correction to the aileron hinge-moment coefficient caused by asymmetrical loading may be expressed roughly as

$$\Delta C_h = -15 \frac{b_a}{A} \frac{\partial C_h}{\partial \alpha} C_l$$

where the value of $\frac{\partial C_h}{\partial \alpha}$ (α in degrees) is determined experimentally (or estimated) for a given model. This correction is very small for models having ordinary proportions.

ILLUSTRATIVE EXAMPLE

The method of computing the jet-boundary corrections for a reflection-plane model will be illustrated in detail by an example. The method applies to any rectangular tunnel but, because the computations of the boundary-induced upwash velocities (figs. 4 and 5) have been performed only for a 7- by 10-foot closed tunnel, the example is for a model in a tunnel of these dimensions.

In practice, however, the principal corrections for models in 7- by 10-foot tunnels can be more easily obtained from the graphs and empirical equations just presented. In practice, also, it will seldom be worth while to compute all the corrections, such as those to the span load distribution; however, for completeness, all the corrections will be computed in the example. It might be noted that it is often convenient to use a single average correction for wing-flap combinations rather than to break the correction into two parts. The accuracy required for the corrections will determine the number of these simplifications that may be used.

The constants for the assumed model (fig. 15) that are required for the computations are as follows:

Aspect ratio, A	6
Taper ratio, λ	0.5
Semispan, $b/2$, feet	7.0
Wing area, S , square feet	32.67
Flap area, S_f , square feet	1.94
Flap-span ratio, $\frac{b_f}{b/2}$	0.5
Flap-chord ratio, c_f/c	0.2
Flap mean chord, \bar{c}_f , foot	0.55
Aileron area, S_a , square feet	1.19
Location, inboard aileron tip, $\frac{y}{b/2}$	0.50
Location, outboard aileron tip, $\frac{y}{b/2}$	0.97
Aileron-chord ratio, c_a/c	0.2
Aileron mean chord, \bar{c}_a , foot	0.40

The wing has rounded tips and is equipped with plain, unbalanced, sealed, constant-percentage-chord flaps and ailerons. The model is mounted on the center line of a 7- by 10-foot wind tunnel.

Because the influence lines of reference 5 are used in the calculations, the slope of the section lift curves used for reference 5 will be used in this example. The value of the slope of the section lift curve a_0 is 5.67 per radian and of the slope of the finite-span lift curve a_1 is 4.38 per radian.

Symmetrical Loading Conditions

Computations for the symmetrical loading conditions may be made in the following steps:

1. Values of $(w/\Gamma)_w$ for the horseshoe vortex repre-

sending the wing are obtained from table II by assuming an effective vortex semispan y_1 of 6.0 feet. The recommended value of y_1 would be $0.88 b/2$, or 6.16 feet, but the nearest $\frac{1}{8}$ -foot value is selected in order to use the numerical values of the upwash velocities from the table without interpolation. The upwash angle at each station for unit lift coefficient is obtained from equation (1) where the single load increment $\Delta \left(\frac{c c_L A}{b C_L} \right)_{y_1 w}$ is equal to $\frac{b/2}{y_1}$ and therefore

$$\left(\frac{w}{\sqrt{C_L}} \right)_w = \left(\frac{w}{\Gamma} \right)_{y_1} \left[\frac{(14)^2}{4 \times 6 \times 6} \right] = 1.361 \left(\frac{w}{\Gamma} \right)_{y_1}$$

The upwash angle is plotted in figure 16.

2. Values of $(w/\Gamma)_f$ for the horseshoe vortex representing the flaps are obtained from table II for a value of y_1 of 4.5 feet, which corresponds approximately to the recommended ratio $b_{f_g}/b_f = 1.29$. The upwash angle is

$$\left(\frac{w}{\sqrt{C_L}} \right)_f = \left(\frac{w}{\Gamma} \right)_{y_1} \left[\frac{(14)^2}{4 \times 4.5 \times 6} \right] = 1.815 \left(\frac{w}{\Gamma} \right)_{y_1}$$

and the numerical values are plotted in figure 16.

3. The free-air span loading of this wing, as obtained from reference 6, is plotted in figure 17. The increment of load due to the jet boundaries is calculated from the upwash-angle values determined in step 1 and the influence lines of reference 5 and is plotted in figure 18. The area under the curve of figure 18 is 0.583, which corresponds to a $(\Delta C_L/C_L)_w$ of $0.583/7$ or 0.0833. The increments of jet-boundary-induced load are multiplied by $1/(1-0.0833)$ or 1.091 and are added to the free-air load and plotted in figure 17. The tunnel loading corresponding to unit lift coefficient is obtained by multiplying the ordinates of the total-load curve by the area ratio $\frac{7.0}{7.0 + 0.583 \times 1.091}$.

A comparison of the final tunnel load curve with the free-air load curve and the span-load data of reference 6 shows that the tunnel loading corresponds to a taper ratio of about 0.45.

4. The same procedure applied to the span-load curve for the flaps, as obtained from reference 5, is illustrated in figures 18 and 19.

5. The values of $\left[\frac{\partial \left(\frac{w}{\Gamma} \right)}{\partial x} \right]_w$ required to compute the corrections due to streamline curvature are taken from table I. The summation product

$$\sum \left[\frac{\partial \left(\frac{w}{\Gamma} \right)}{\partial x} \right]_{y_{1w}} \Delta \left(\frac{cc_l A}{bC_L} \right)_{y_{1w}}$$

for the wing corresponds to a one-step approximation to the load curve as shown in figure 20. The value of

$\Delta \left(\frac{cc_l A}{bC_L} \right)_{y_{1w}}$ for $y_1 = 6$ is 1.167. The results of the cal-

culatior of the desired product

$$\frac{2A}{b} \left[\frac{\partial \left(\frac{w}{\sqrt{C_L}} \right)}{\partial x} \right]_w c^3 = c^3 \sum \left[\frac{\partial \left(\frac{w}{\Gamma} \right)}{\partial x} \right]_{y_{1w}} \Delta \left(\frac{cc_l A}{bC_L} \right)_{y_{1w}}$$

are given in figure 21.

6. The product $\frac{2A}{b} \left[\frac{\partial \left(\frac{w}{\sqrt{C_L}} \right)}{\partial x} \right]_f c^3$ for the flap is found similarly. The two-step approximation to the load curve is shown in figure 20 and the numerical values of the final product are given in figure 21.

7a. The correction to the angle of attack due to the effect of the jet boundaries on the wing alone is the sum of the corrections obtained from equations (3) and (5). The value of $(\Delta C_L / C_L)_w$ in equation (3) is 0.0833 as found in step 3. Thus, from equation (3),

$$\Delta \alpha_w = \frac{0.0833 \times 57.3}{4.38} C_{Lw} = 1.090 C_{Lw}$$

The factor $0.50 - \frac{x_{l.l.}}{c}$ of equation (5) may be assumed to be equal to 0.25 for the wing alone and

$$\int_0^{b/2} \frac{2A}{b} \left[\frac{\partial \left(\frac{w}{vC_L} \right)}{\partial x} \right]_w c^2 dy = 0.248$$

from a mechanical integration of the curve in figure 21. (The moment of the area about the plane of symmetry is found at this time to be 0.580 and will be used in step 14.) Thus

$$(\Delta\alpha_{s.c.})_w = \frac{57.3 \times 0.25 C_{L_w}}{14} \times 0.248 = 0.254 C_{L_w}$$

7b. The alternate method of obtaining the angle-of-attack correction is given in equation (4). Figure 22 gives values of $\left(\frac{w}{vC_L} \right) c$ for the wing. The area under the curve is equal to 0.307, which gives a correction equal to

$$\Delta\alpha_w = \frac{57.3 C_{L_w} \times 2 \times 0.307}{32.57} = 1.078 C_{L_w}$$

The value of $(\Delta\alpha_{s.c.})_w$ will, of course, be the same as found in step 7a.

8. The total angle-of-attack correction due to the wing alone is, from step 7a,

$$\Delta\alpha_w = 1.090 C_{L_w} + 0.254 C_{L_w} = 1.344 C_{L_w}$$

or, from step 7b,

$$\Delta\alpha_w = 1.078 C_{L_w} + 0.254 C_{L_w} = 1.332 C_{L_w}$$

9. The correction to the angle of attack due to the flap loading is found, from equation (3), to be

$$\Delta\alpha_f = 1.200 C_{L_f}$$

or, from equation (4),

$$\Delta\alpha_f = 1.190 C_{L_f}$$

The effect of streamline curvature is not considered because the factor $0.50 - \frac{x_{l.l.}}{c} \approx 0$ for the flapped wing.

10. The total correction to the angle of attack is

the sum of the wing and flap corrections, from equations (3) and (5),

$$\Delta\alpha_{total} = \Delta\alpha_w + \Delta\alpha_f = 1.34 C_{Lw} + 1.20 C_{Lf}$$

or, from equations (4) and (5)

$$\Delta\alpha_{total} = 1.33 C_{Lw} + 1.19 C_{Lf}$$

11. The correction to the lift of the wing is given in equation (7) as

$$(\Delta C_{L_{s.c.}})_w = -0.254 C_{Lw} \frac{4.38}{57.3} = -0.0194 C_{Lw}$$

12. The correction to the lift of the flap is computed from equation (6) as

$$(\Delta C_{L_{s.c.}})_f = -\frac{4.38 C_{Lf}}{4(14)} (0.267) = -0.0209 C_{Lf}$$

13. The total lift correction is

$$(\Delta C_{L_{s.c.}})_{total} = -0.0194 C_{Lw} - 0.0209 C_{Lf}$$

14. The moments of area determined in steps 7 and 13 will be used in the determination of the spanwise center of pressure of the lift correction load from equation (9), which gives a value of $\bar{y}_{s.c.} = 2.36$ feet for the wing correction and $\bar{y}_{s.c.} = 2.16$ feet for the flap correction. These values are required for the computation of the correction to the pitching-moment coefficient.

15. The correction to the measured pitching moment due to the wing alone is obtained from equation (8) where the chord c at the lateral center of pressure determined in step 14 is 2.64 feet. Because the pitching-moment coefficients for this model are given about the 0.25c line and in terms of the mean chord, $x_{cm} = 2.64/4$ and $\bar{c}_w = S/b = 2.333$. The correction as obtained from equation (8) is

$$\begin{aligned} (\Delta C_{m_{s.c.}})_w &= \frac{2.64}{4} \frac{5.67 C_{Lw}}{2.333 \times 4 \times 14} 0.248 \\ &= 0.0071 C_{Lw} \end{aligned}$$

L-158

16. The correction to the flap pitching moment is found by the same method to be

$$(\Delta C_{m_{s.c.}})_f = 0.0077 C_{L_f}$$

17. The total pitching-moment-coefficient correction is

$$\Delta C_{m_{s.c.}} = 0.0071 C_{L_w} + 0.0077 C_{L_f}$$

18. The induced-drag-coefficient correction is determined from equations (11) and (12) and the integrals of the various products of boundary-induced upwash and load parameters are obtained in steps 1 to 4 and are plotted in figure 23. Thus,

$$\begin{aligned} \Delta C_{D_i} &= \frac{2}{14} \left[0.132 C_{L_w}^2 + 0.169 C_{L_f}^2 + (0.145 + 0.144) C_{L_w} C_{L_f} \right] \\ &= 0.0189 C_{L_w}^2 + 0.0241 C_{L_f}^2 + 0.0413 C_{L_w} C_{L_f} \end{aligned}$$

19. The induced-yawing-moment-coefficient correction, obtained from equations (12) and (13) and the moment integrals of figure 23, is

$$\begin{aligned} \Delta C_{n_1} &= - \frac{1}{(14)^2} \left[0.340 C_{L_w}^2 + 0.306 C_{L_f}^2 + (0.286 + 0.330) C_{L_w} C_{L_f} \right] \\ &= -0.0017 C_{L_w}^2 - 0.0016 C_{L_f}^2 - 0.0031 C_{L_w} C_{L_f} \end{aligned}$$

20. The correction to the flap and aileron hinge-moment coefficients due to streamline curvature is given in equation (17). The value of F from figure 8 is 0.036. Mechanical integration of the curves of figure 24 gives for the corrections to the flap hinge-moment coefficient

$$\Delta C_{h_f} = \frac{5.67 \times 14 \times 0.036}{8\pi \times 6 \times 1.94 \times 0.55} (0.502 C_{L_w} + 0.602 C_{L_f})$$

or

$$\Delta C_{h_f} = 0.0089 C_{L_w} + 0.0107 C_{L_f}$$

The value of the correction determined from figure 14 is somewhat smaller ($\Delta C_{h_f} = 0.0083 C_L$), because the chords

near the root sections are smaller for the wings of reference 5 than for wings with linear taper. The correction to the aileron hinge-moment coefficient is

$$\Delta C_{ha} = \frac{5.67 \times 14 \times 0.036}{8\pi \times 6 \times 1.19 \times 0.40} (0.137 C_{Lw} + 0.115 C_{Lf})$$

$$\Delta C_{ha} = 0.0051 C_{Lw} + 0.0046 C_{Lf}$$

Asymmetrical Loading Conditions

21. The free-air span load distribution due to the deflection of one aileron is obtained from reference 5 in terms of $cc_l/c_s\alpha$ and is plotted in figure 25(a). The loading in terms of the parameter cc_lA/bC_{l_c} is obtained by so adjusting the ordinates of the curve of figure 25(a) that the moment of area about the plane of symmetry is equal to $4.0 (b/2)^2$. The conversion may be made graphically or by means of equation (18) where $c_sA/b = 1.37$ from figure 6 and, from figure 16 of reference 5, the value of C_{l_δ}/k is the difference between the values at

$$\frac{y}{b/2} = 0.97 \quad \text{and at} \quad \frac{y}{b/2} = 0.5, \quad \text{that is,}$$

$$C_{l_\delta}/k = 0.73 - 0.25 = 0.48$$

and

$$C_{l_c}/\alpha = 0.5 C_{l_\delta}/k = 0.24$$

Therefore

$$\frac{cc_lA}{bC_{l_c}} = \frac{1.37}{0.24} \frac{cc_l}{c_s\alpha} = 5.70 \frac{cc_l}{c_s\alpha}$$

The new curve of free-air load is plotted in figure 25(b). The reflection load is added to the free-air load to give the reflection-loading curve of figure 25(b). The jet-boundary-induced upwash angle is obtained from equation (2) for the three-step approximation to the load curve (as indicated in fig. 25(b)). The numerical values of

$$\left[\frac{w}{\sqrt{C_{l_c} + 2\Delta C_{l_r}}} \right]_i$$

are plotted in figure 26. The corre-

sponding increment of load at each spanwise station is ob-

L-458

tained from the influence lines of reference 5 and is presented in figure 27. The increment presented in figure 27 must be divided by

$$1 - \frac{\Delta C_l}{1 + \frac{2\Delta C_{l_r}}{C_{l_c}}}$$

where ΔC_l is obtained from equation (21) and the moment of the curve of figure 27 as

$$\Delta C_l = \frac{10.73}{(14)^3} = 0.0547$$

and $1 + \frac{2\Delta C_{l_r}}{C_{l_c}}$ is equal to 1.084 from figure 9. The corrected increments are added to the reflection-load curves of figure 25(b) to give the tunnel-load curve (fig. 25(c)) at the same aileron angle as the curve for the free-air load. The ordinates are again adjusted to give a moment of $4.0 (b/2)^3$, which corresponds to unit rolling-moment coefficient. The resulting corrected tunnel-load curve is presented in figure 25(c).

22a. The corrected rolling-moment coefficient is obtained from equation (20) where

$$1 + \frac{2\Delta C_{l_r}}{C_{l_c}} = 1.084$$

and, from step 21,

$$\Delta C_l = 0.0547$$

$$C_{l_c} = \frac{C_l \left[1 - \frac{0.0547}{1.084} \right]}{1.084} = 0.876 C_l$$

22b. The alternate method of determining the corrected rolling-moment coefficient is to use equation (19) to calculate ΔC_l . The product $\left[\frac{w}{V(C_{l_c} + 2\Delta C_{l_r})} \right]^2 c$ is plot-

ted in figure 28 and the area moment is found by mechanical integration to be 5.848. Figure 10 gives $J = 1.93$. Therefore,

$$\Delta C_l = \frac{(6)^2 \times 5.67}{(14)^3 \times (6 + 1.93)} \times 5.848 = 0.0547$$

which is the same, in this case, as the value calculated in step 21. The agreement usually will be close but not necessarily exact.

23. The correction to the yawing-moment coefficient due to aileron deflection is obtained from equation (22). For this model the value of $(\Delta C_{n1})_1$, due to the absent wing, is found from figure 11 to be $-0.0104 C_{l_c} C_L$. Step 22a gave $C_{l_c} = 0.876 C_l$. Thus: $(\Delta C_{n1})_1 = -0.0090 C_l C_L$. By considering the aileron-wing combination and using $(w/\sqrt{C_L})_w$ from figure 16, $\left[\frac{w}{\sqrt{C_{l_c} + 2\Delta C_{l_r}}} \right]'$ from figure 26, tunnel $(cc_l A/bC_L)_w$ from figure 17, and tunnel $cc_l A/bC_{l_c}$ from figure 25(c), equation (13) gives

$$(\Delta C_{n1})_2 = - \frac{C_{L_w} C_l}{b^2 \left(1 + \frac{2\Delta C_{l_r}}{C_{l_c}} \right)} \int_0^{b/2} \left[\frac{w}{\sqrt{C_{l_c} + 2\Delta C_{l_r}}} \right]' \left(\frac{cc_l A}{bC_L} \right)_w y dy$$

and

$$(\Delta C_{n1})_3 = - \frac{C_{L_w} C_l}{b^2} \int_0^{b/2} \left(\frac{w}{\sqrt{C_L}} \right) \frac{cc_l A}{bC_{l_c}} y dy$$

The aileron-flap combinations are determined similarly.

The products of the various upwash and loading parameters are plotted in figure 29 and mechanical moment integrations give

$$(\Delta C_{n1})_2 = - \frac{2.442}{b^2 \left(1 + \frac{2\Delta C_{l_r}}{C_{l_c}} \right)} C_{L_w} C_l$$

L-458

40

$$(\Delta C_{n1})_3 = - \frac{2.925}{b^2} C_{LW} C_l$$

$$(\Delta C_{n1})_4 = - \frac{1.680}{b^2 \left(1 + \frac{2\Delta C_{lr}}{C_{lc}} \right)} C_{L_f} C_l$$

$$(\Delta C_{n1})_5 = - \frac{2.517}{b^2} C_{L_f} C_l$$

When it is known that $b = 14$ feet and $1 + \frac{2\Delta C_{lr}}{C_{lc}} = 1.084$ the total correction to the yawing-moment coefficient as obtained from equation (22) is

$$\Delta C_{n1} = -0.009 C_L C_l - 0.026 C_{LW} C_l - 0.021 C_{L_f} C_l$$

25. The second component of the aileron hinge-moment correction is obtained approximately from equation (23), with the use of figures 37 and 25(b). The total increment of load at the aileron center section is

$$\Delta \left[\frac{c c_l A}{b(C_{lc} + 2\Delta C_{lr})} \right] + \Delta \left(\frac{c c_l A}{b C_{lc}} \right) = 0.45 + 0.25 = 0.70$$

From reference 9

$$\frac{\partial c_h}{\partial c_n} = -0.265 c_f / c$$

Therefore, the correction is

$$\Delta C_h \approx - \frac{14 C_l}{2.0 \times 6.0} (-0.265) (0.2) (0.70) = 0.04 C_l$$

CONCLUDING REMARKS

The method for determining the jet-boundary corrections for reflection-plane models in rectangular wind tunnels was presented in some detail in order to make the method as routine as possible. The method includes the determination

L-458

of the tunnel span load distribution and the derivation of equations giving the corrections to the angle of attack, the lift and drag coefficients, and the pitching-, rolling-, yawing-, and hinge-moment coefficients. The principal effects of aerodynamic induction and the curvature of the streamlines have been considered.

Numerical values of the more important corrections were calculated for a series of representative models mounted in 7- by 10-foot closed rectangular wind tunnels. In order to simplify the calculation of corrections for models of unusual size in 7- by 10-foot closed wind tunnels, tables of the numerical values of the jet-boundary-induced upwash were presented.

Langley Memorial Aeronautical Laboratory,
National Advisory Committee for Aeronautics,
Langley Field, Va.

REFERENCES

1. Glauert, H.: The Interference of Wind Channel Walls on the Aerodynamic Characteristics of an Aerofoil. R. & M. No. 867, British A.R.C., 1923.
2. Swanson, Robert S., and Schuldenfrei, Marvin J.: Jet-Boundary Corrections to the Downwash behind Powered Models in Rectangular Wind Tunnels with Numerical Values for 7- by 10-Foot Closed Wind Tunnels. NACA A.R.E., Aug. 1942.
3. Theodorsen, Theodore: The Theory of Wind-Tunnel Wall Interference. Rep. No. 410, NACA, 1931.
4. Theodorsen, Theodore: Interference on an Airfoil of Finite Span in an Open Rectangular Wind Tunnel. Rep. No. 461, NACA, 1933.
5. Pearson, Henry A., and Jones, Robert T.: Theoretical Stability and Control Characteristics of Wings with Various Amounts of Taper and Twist. Rep. No. 635, NACA, 1938.
6. Anderson, Raymond F.: Determination of the Characteristics of Tapered Wings. Rep. No. 572, NACA, 1936.
7. Pearson, H. A.: Span Load Distribution for Tapered Wings with Partial-Span Flaps. Rep. No. 585, NACA, 1937.
8. Millikan, Clark B.: On the Lift Distribution for a Wing of Arbitrary Plan Form in a Circular Wind Tunnel. A.S.M.E. Trans., APM-54-19, vol. 54, no. 18, Sept. 30, 1932, pp. 197-203.
9. Ames, Milton B., Jr., and Sears, Richard I.: Determination of Control-Surface Characteristics from NACA Blain-Flap and Tab Data. Rep. No. 721, NACA, 1941.

TABLE I

BOUNDARY INDUCED UPWASH VELOCITY BEHIND LIFTING LINE
 DUE TO SINGLE UNIT COUNTERCLOCKWISE VORTEX ON
 TUNNEL CENTER LINE AND AT TWO DISTANCES y_1 FROM
 REFLECTION PLANE IN 7- BY 10-FOOT
 CLOSED RECTANGULAR WIND TUNNELS

L-458

x y	0	0.5	1.5	3.0	6.0	9.0	$\frac{\partial}{\partial x} \left(\frac{w}{U} \right)$ at $x=0$
$y_1 = 3$							
0	0.01325	0.01533	0.01935	0.02397	0.02805	0.02861	0.00412
2	.01096	.01277	.01616	.02003	.02361	.02394	.00362
4	.00588	.00700	.00906	.01146	.01363	.01380	.00222
6	.00146	.00194	.00281	-----	-----	-----	.00096
8	-.00037	-.00018	.00024	-----	-----	-----	.00036
$y_1 = 6$							
0	0.01706	0.01997	0.02541	0.03193	0.03787	0.03821	0.00588
2	.01605	.01880	.02401	.03018	.03613	.03618	.00550
4	.01286	.01521	.01957	.02565	.02923	.02962	.00472
6	.00827	.00994	.01296	-----	-----	-----	.00334
8	.00551	.00666	.00882	-----	-----	-----	.00230

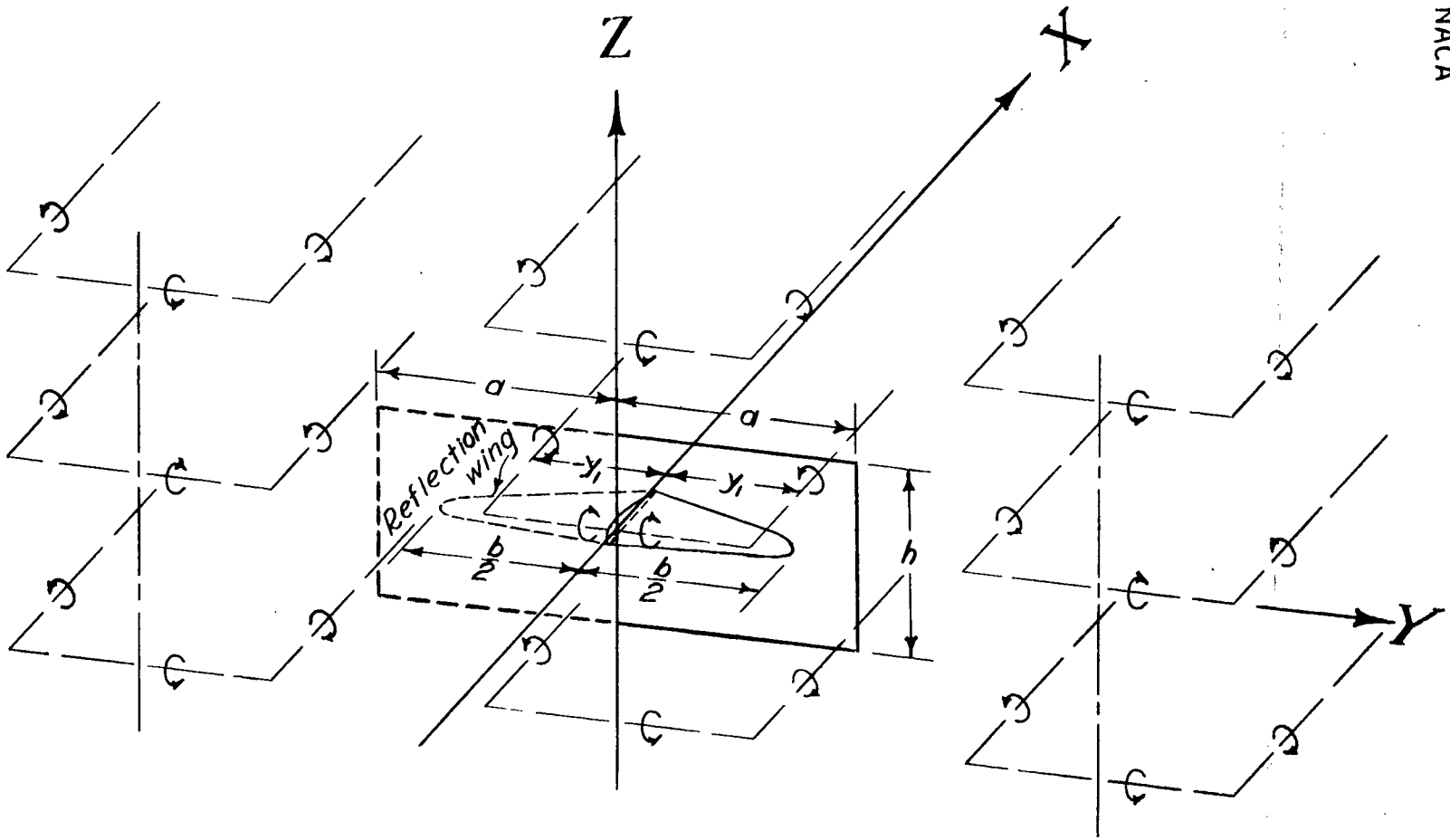


Figure 1.- Three-dimensional arrangement of the doubly infinite image pattern satisfying the boundary conditions for a reflection-plane model of a wing on the center line of a closed rectangular wind tunnel.

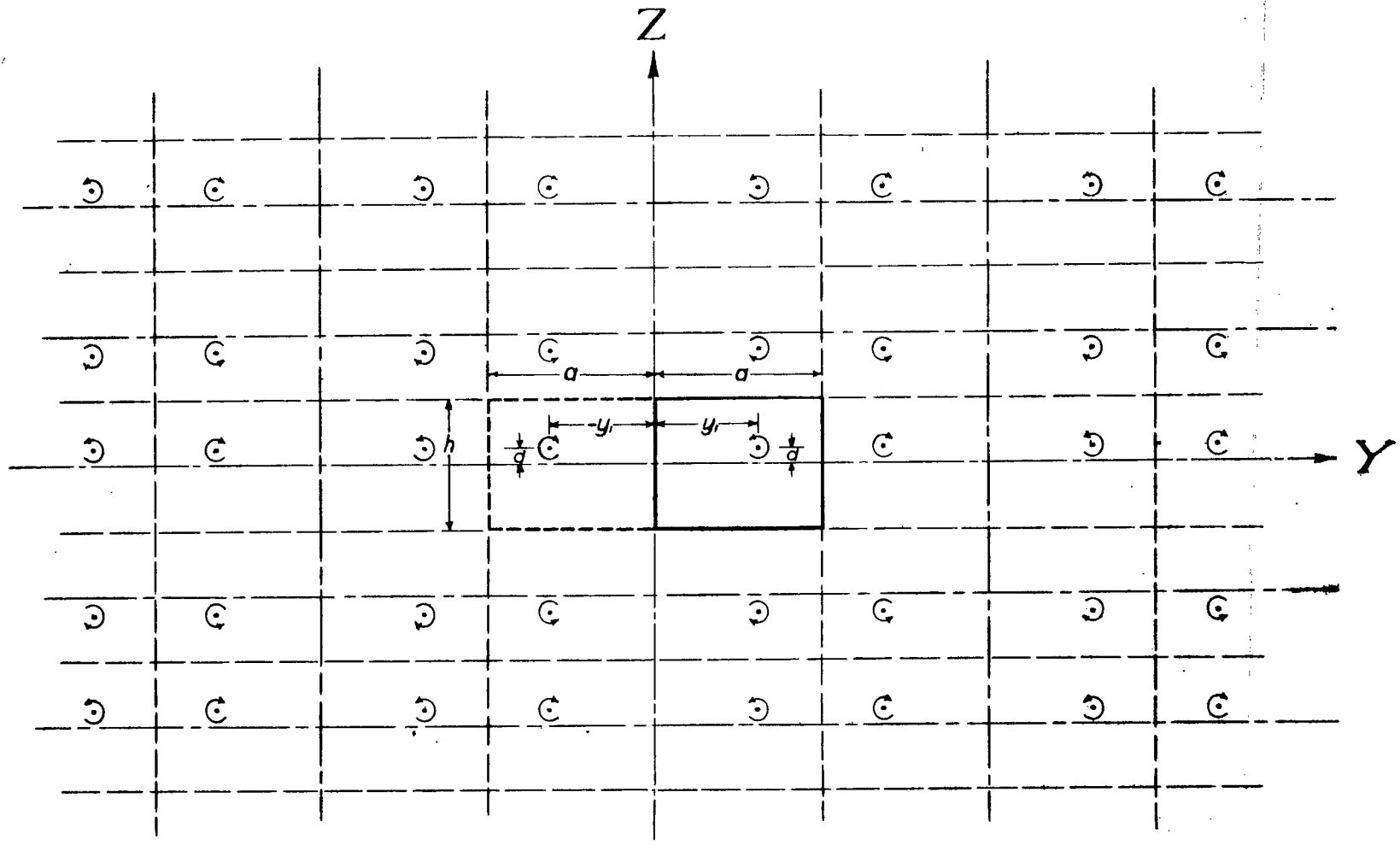


Figure 2.- Two-dimensional arrangement of the infinite image pattern satisfying the boundary conditions for a single trailing vortex and its reflection located above the center line of a closed rectangular wind tunnel.

NACA

Fig. 3

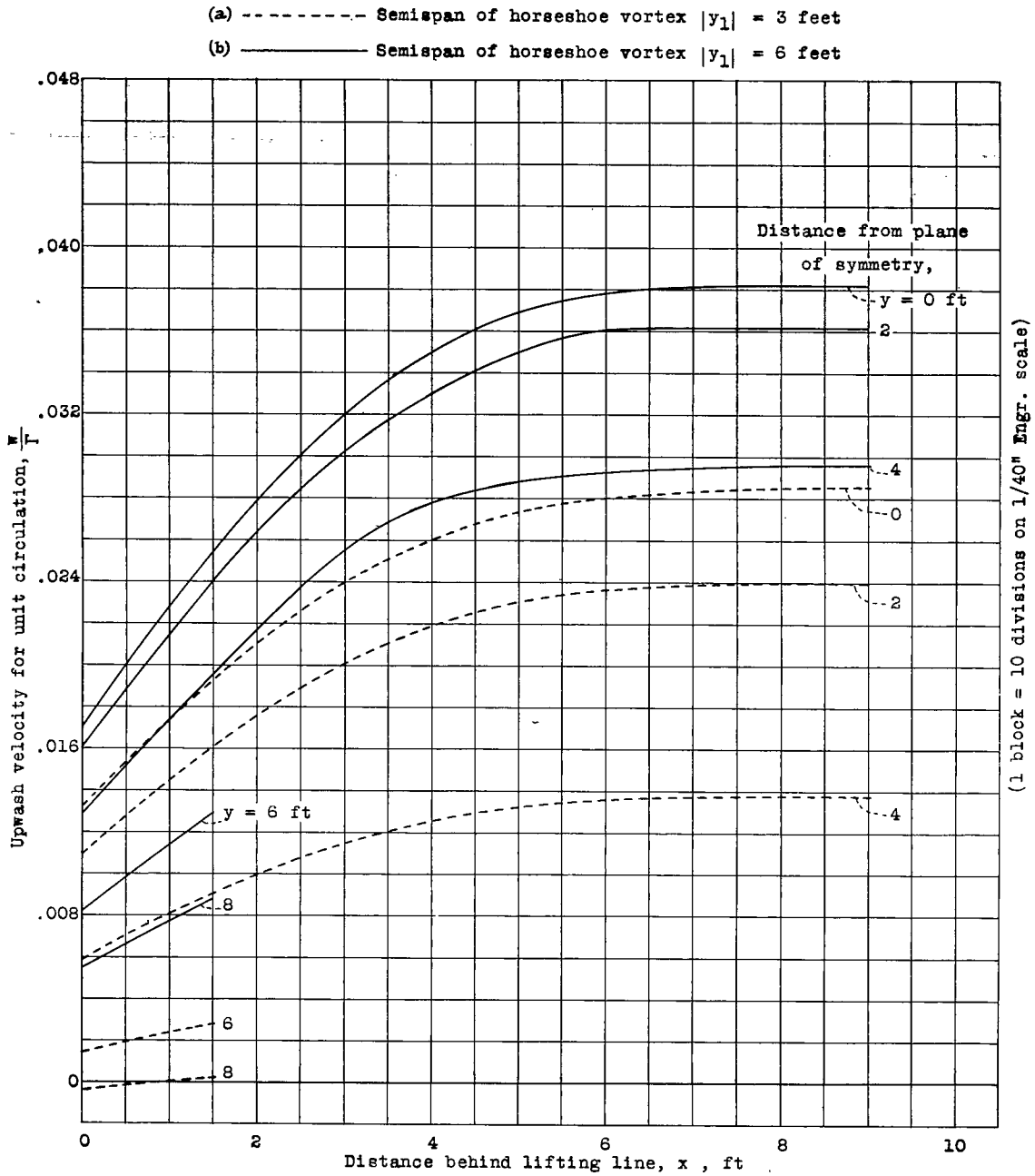


Figure 3.- Boundary-induced upwash velocity behind the lifting line for reflection-plane models mounted in 7- by 10- foot closed rectangular wind tunnels. $d = 0$.

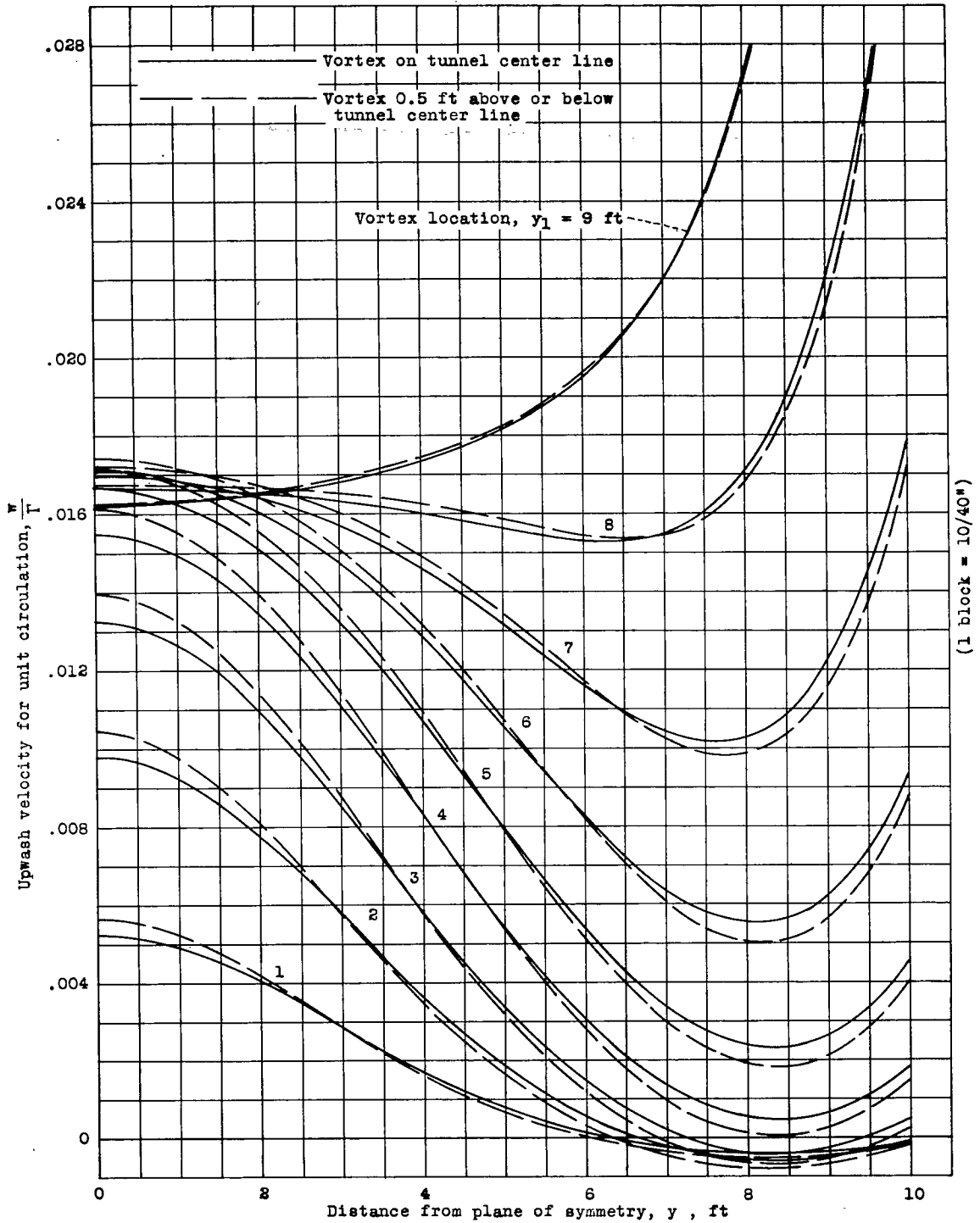


Figure 4.- Boundary-induced upwash velocity at the lifting line due to a single counterclockwise trailing vortex located at various distances y_1 , from the reflection plane in 7-by 10-foot closed rectangular wind tunnels.

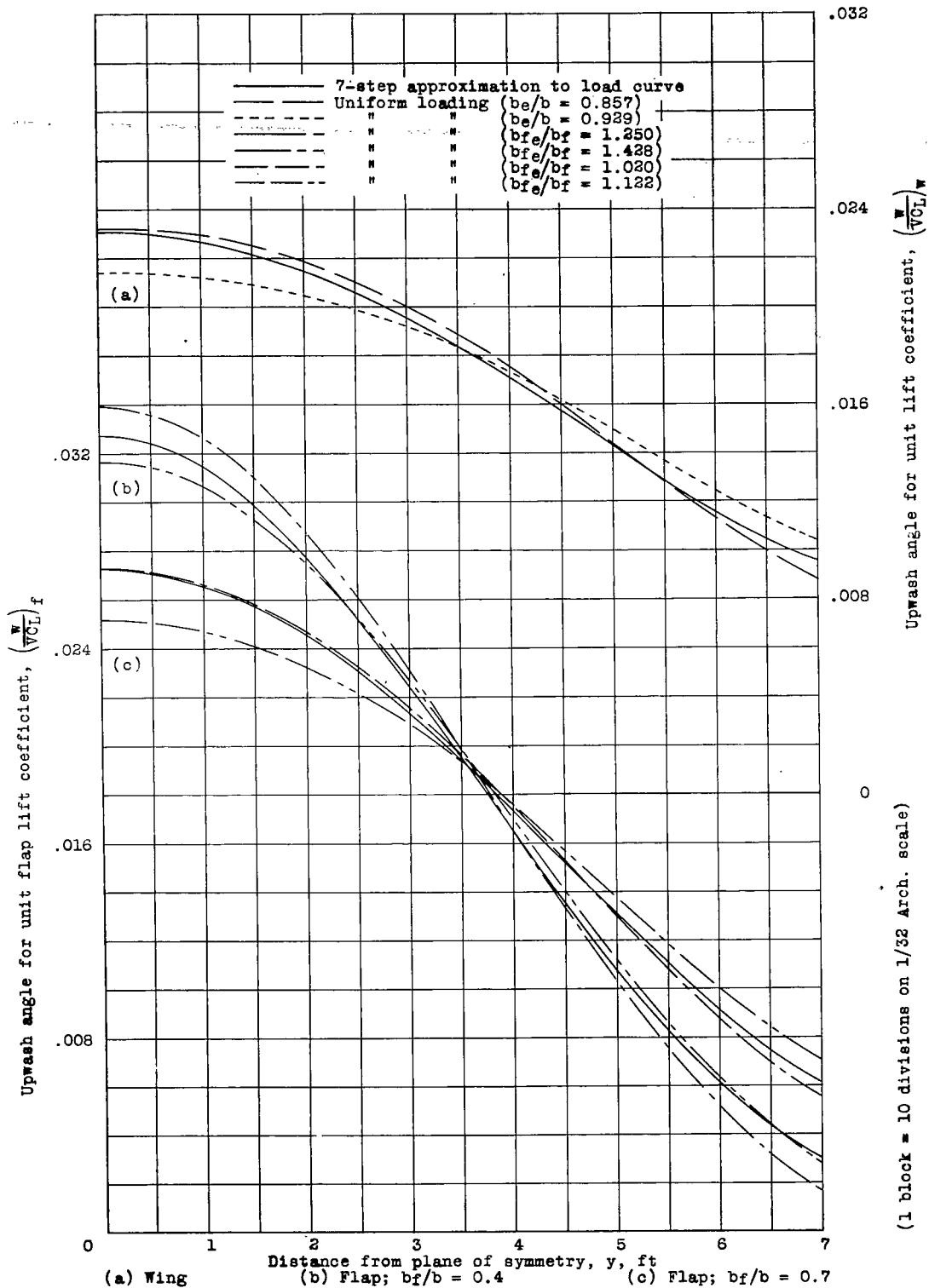


Figure 5.- Boundary-induced upwash angle along the span of a reflection-plane model in a 7-by 10-foot closed rectangular wind tunnel. $b/2 = 7$ feet; $\Lambda = 6$; $\lambda = 0.5$.

NACA

Fig. 6

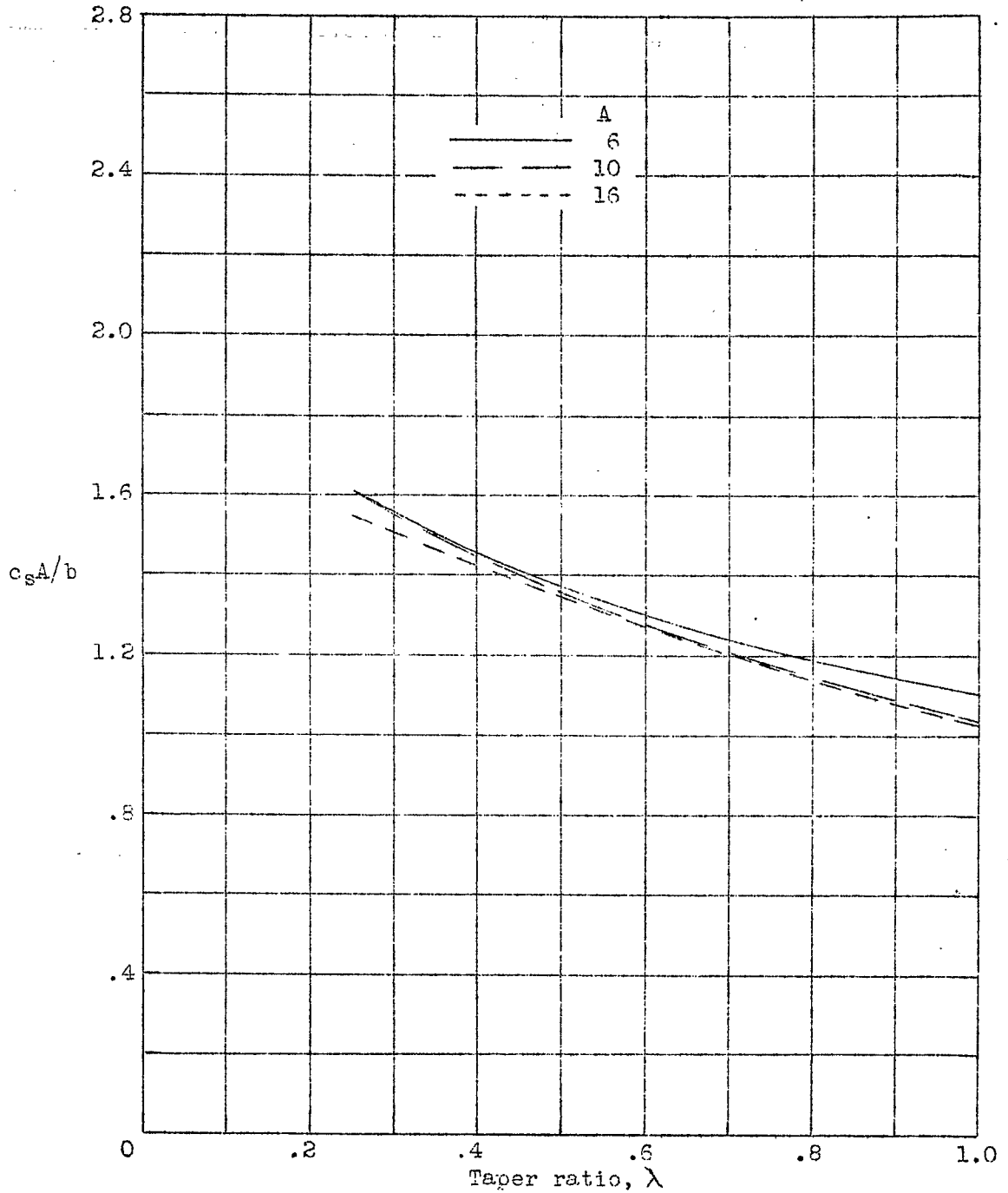
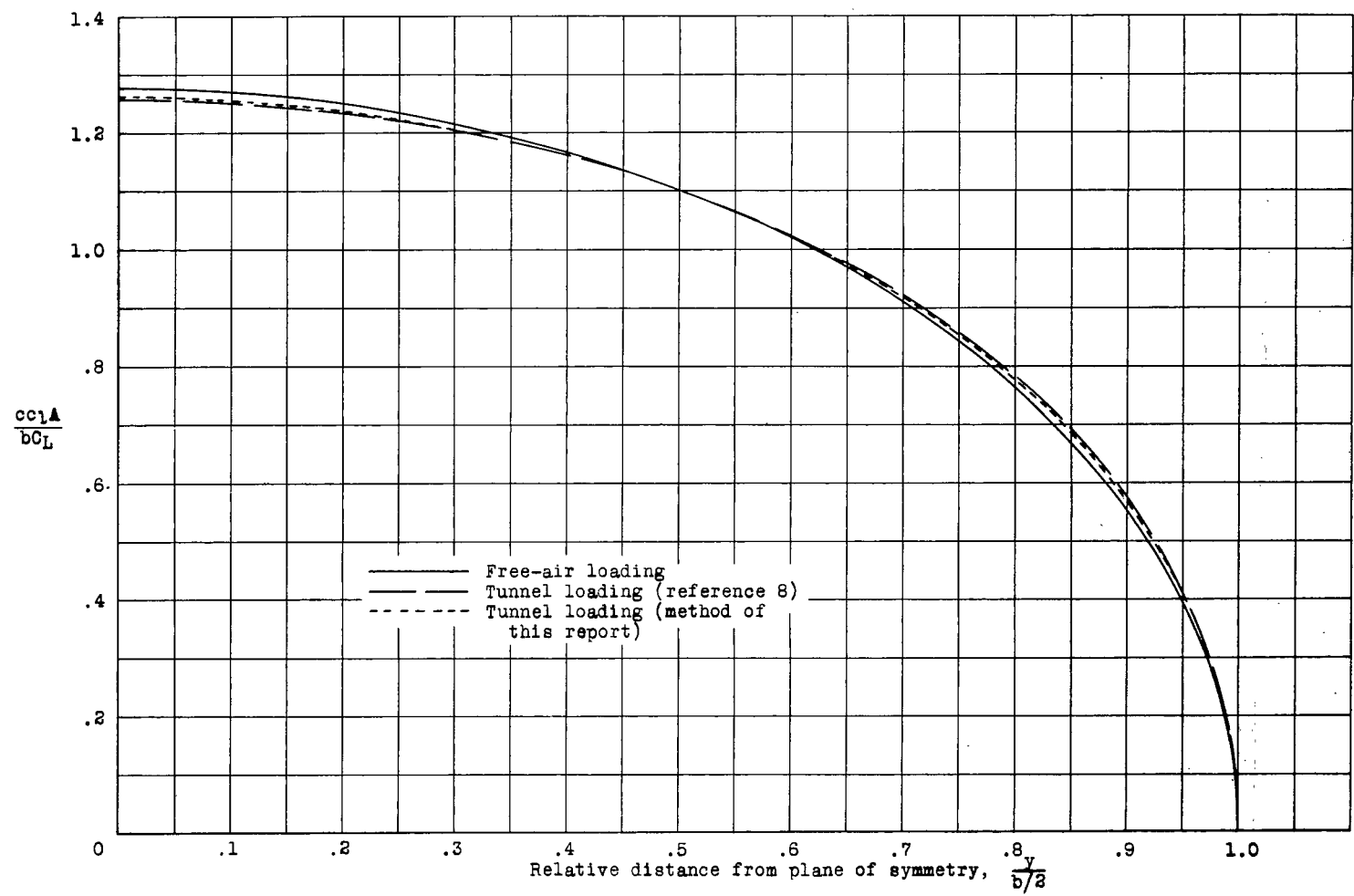


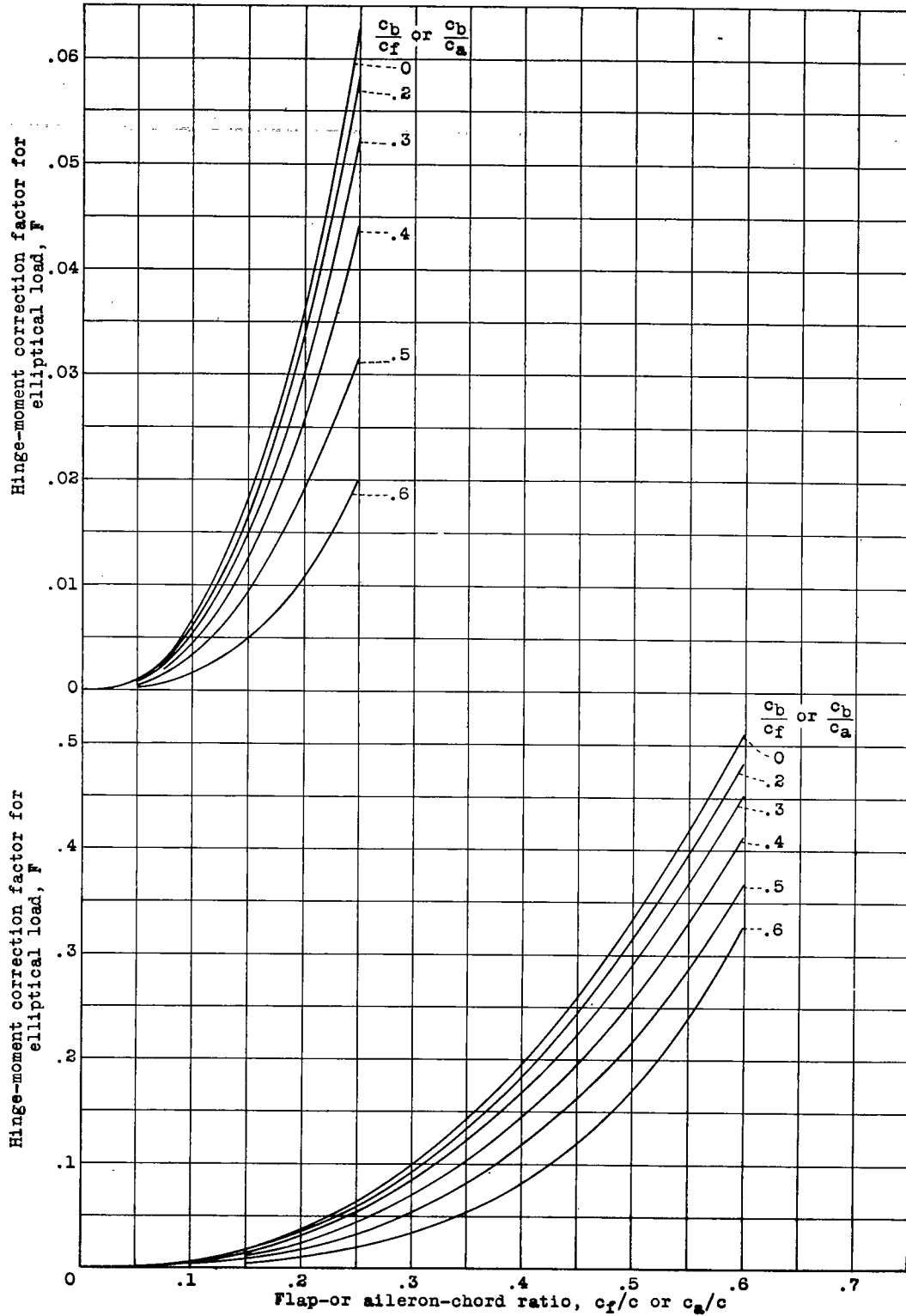
Figure 6.- Values of c_{sA}/b to be used in converting the load parameter cc_1/c_{s0} of reference 5 to the load parameter cc_1A/bc .

L-458



(1 block = 10 divisions on 1/80 Engr. scale)

Figure 7.- Span load distributions for an elliptical wing in free air and in a closed circular tunnel. Wing span is 0.9 times the tunnel diameter.



(1 block = 10/30")

Figure 8.- Variation of the hinge-moment correction factor for elliptical load F with the flap-or aileron-chord ratio c_f/c or c_a/c and the balance-chord ratio c_b/c_f or c_b/c_a .

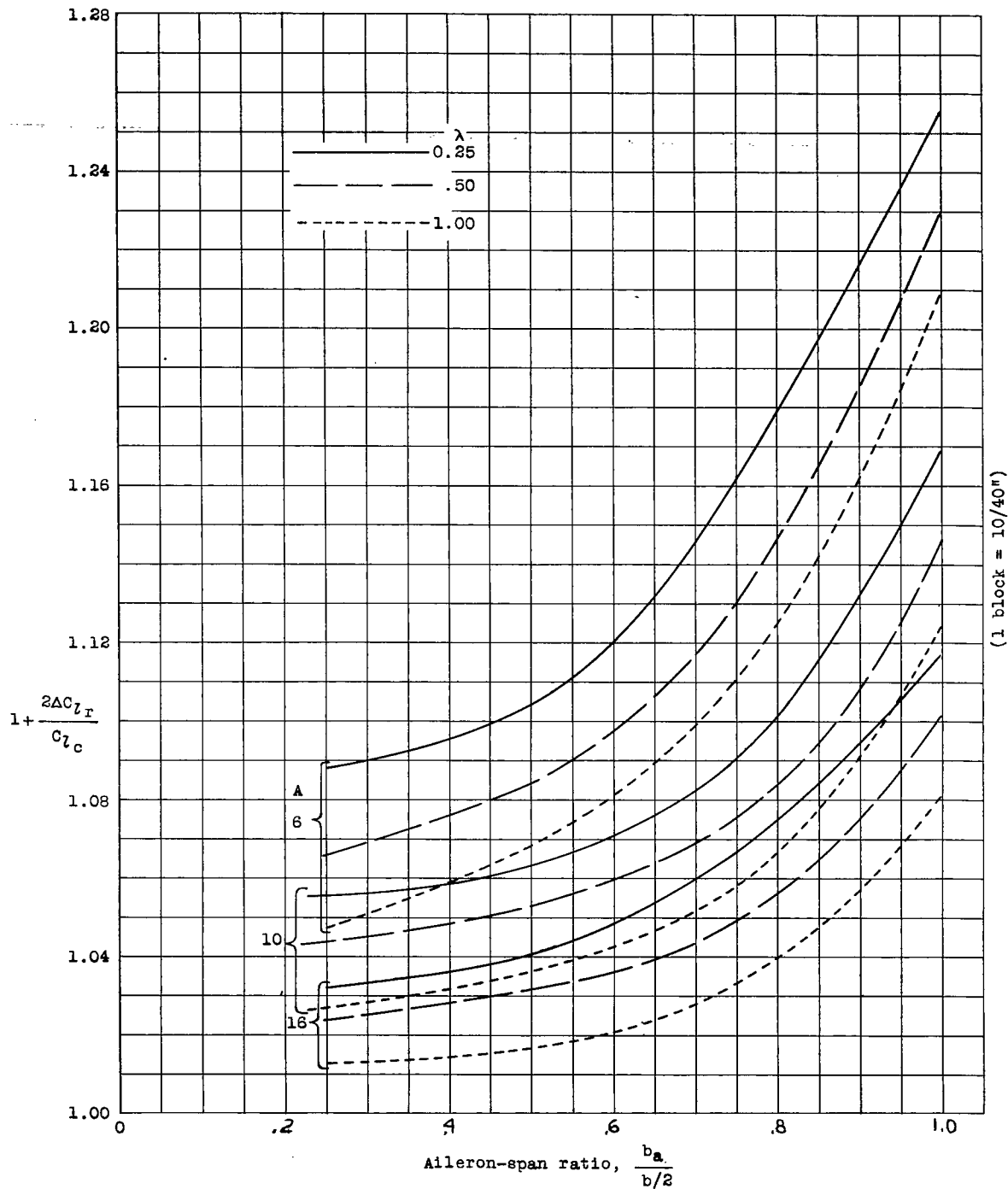


Figure 9.- Values of the factor $1 + \frac{2\Delta C_{l_r}}{C_{l_c}}$ used to account for the effect of the reflection plane on the rolling-moment coefficient for ailerons extending inward from the tips of the wings of reference 5.

85458

NACA

Fig. 10

L-458

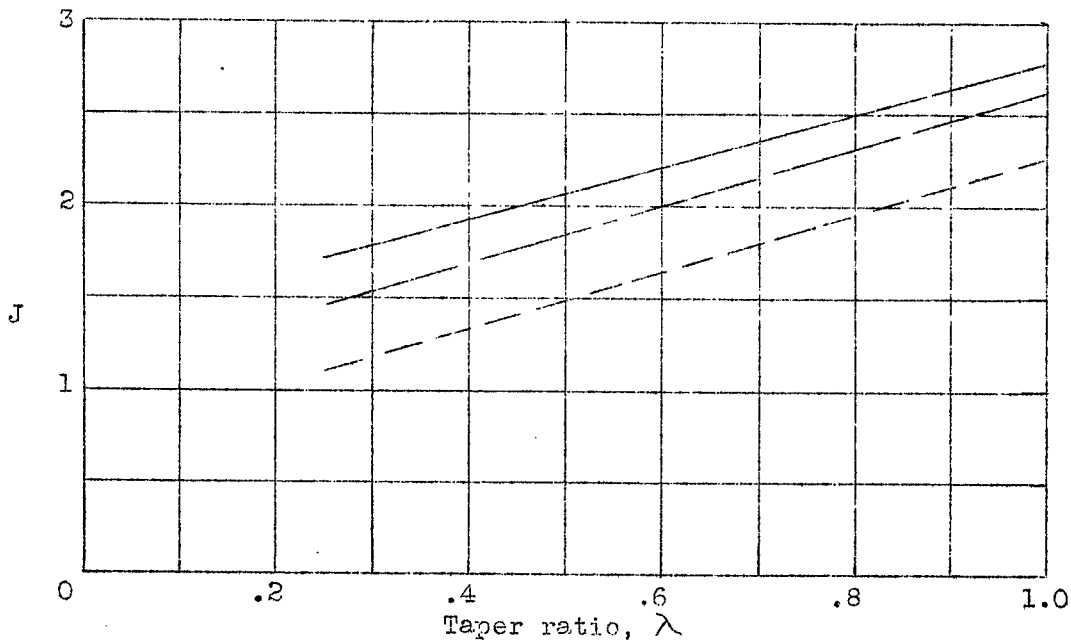
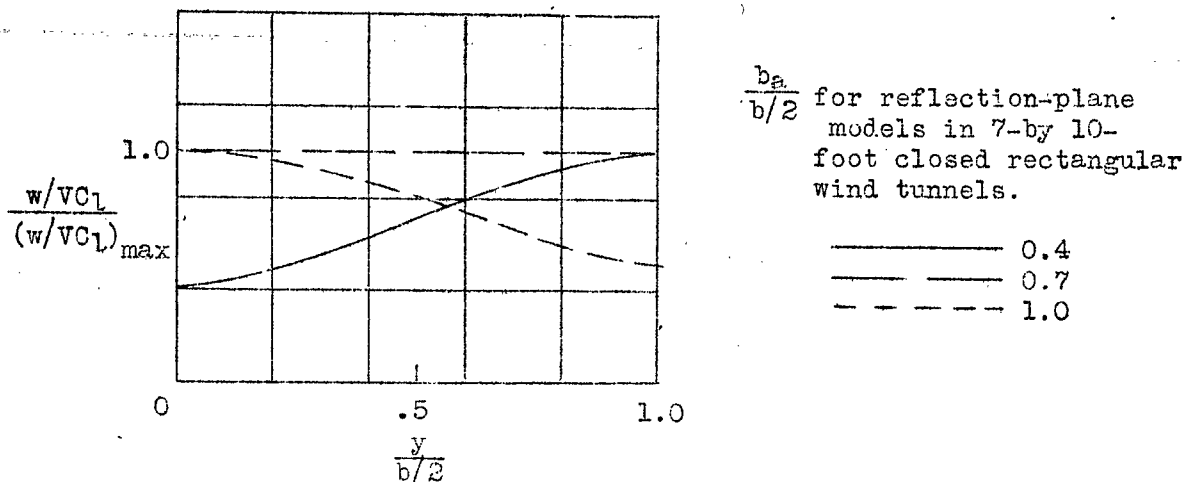


Figure 10.- Values of the aerodynamic-induction factor J used to calculate the rolling-moment correction for asymmetrically loaded reflection-plane models for three different variations of boundary-induced upwash angle. These upwash-angle variations correspond closely to those for aileron-span ratios of 0.4, 0.7, and 1.0 for models in 7-by 10-foot closed rectangular wind tunnels.

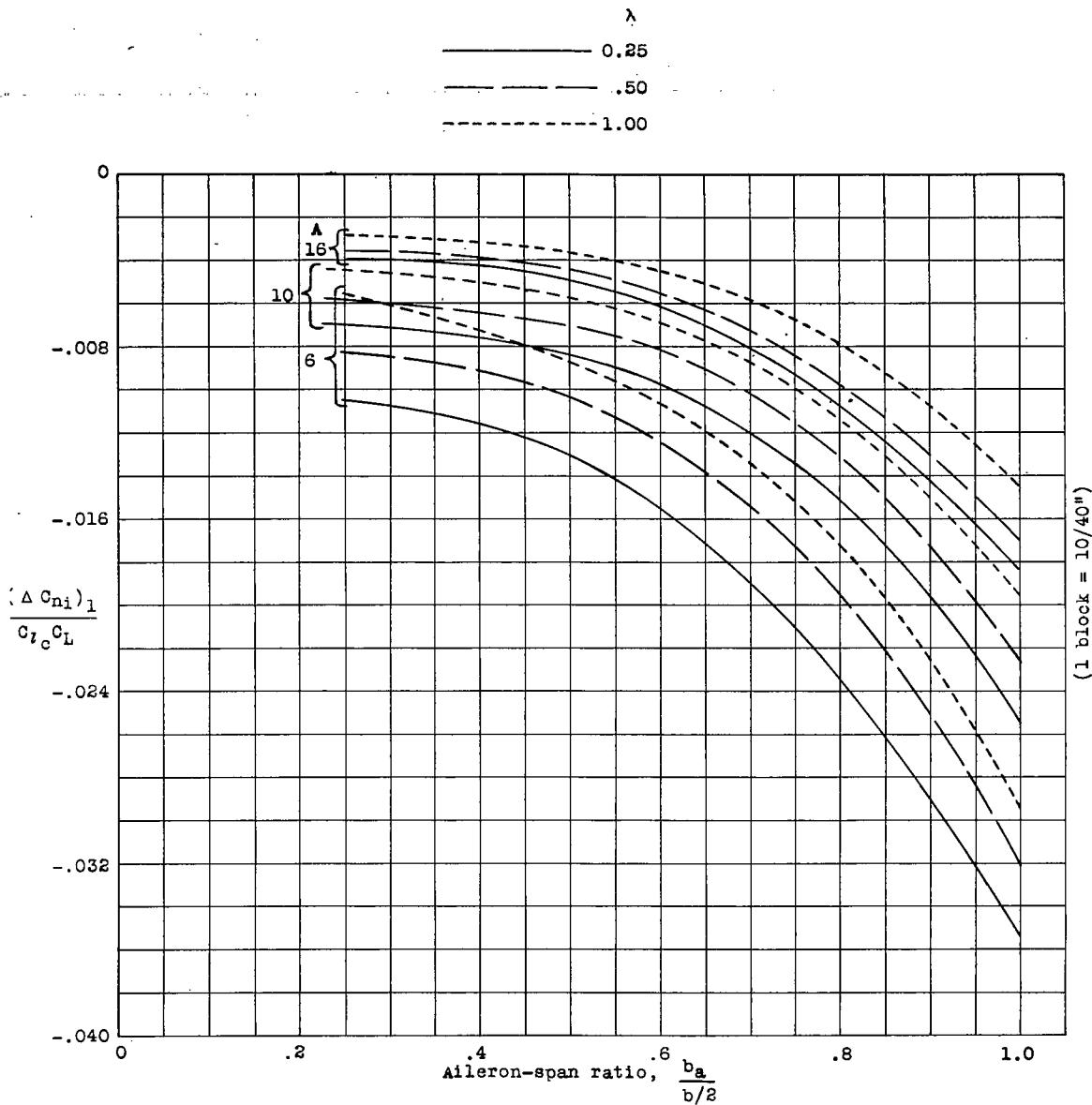


Figure 11.- Increment of yawing-moment correction due solely to the reflection plane for ailerons extending inward from the tips of the wings of reference 5.

NACA

Fig. 12a,b

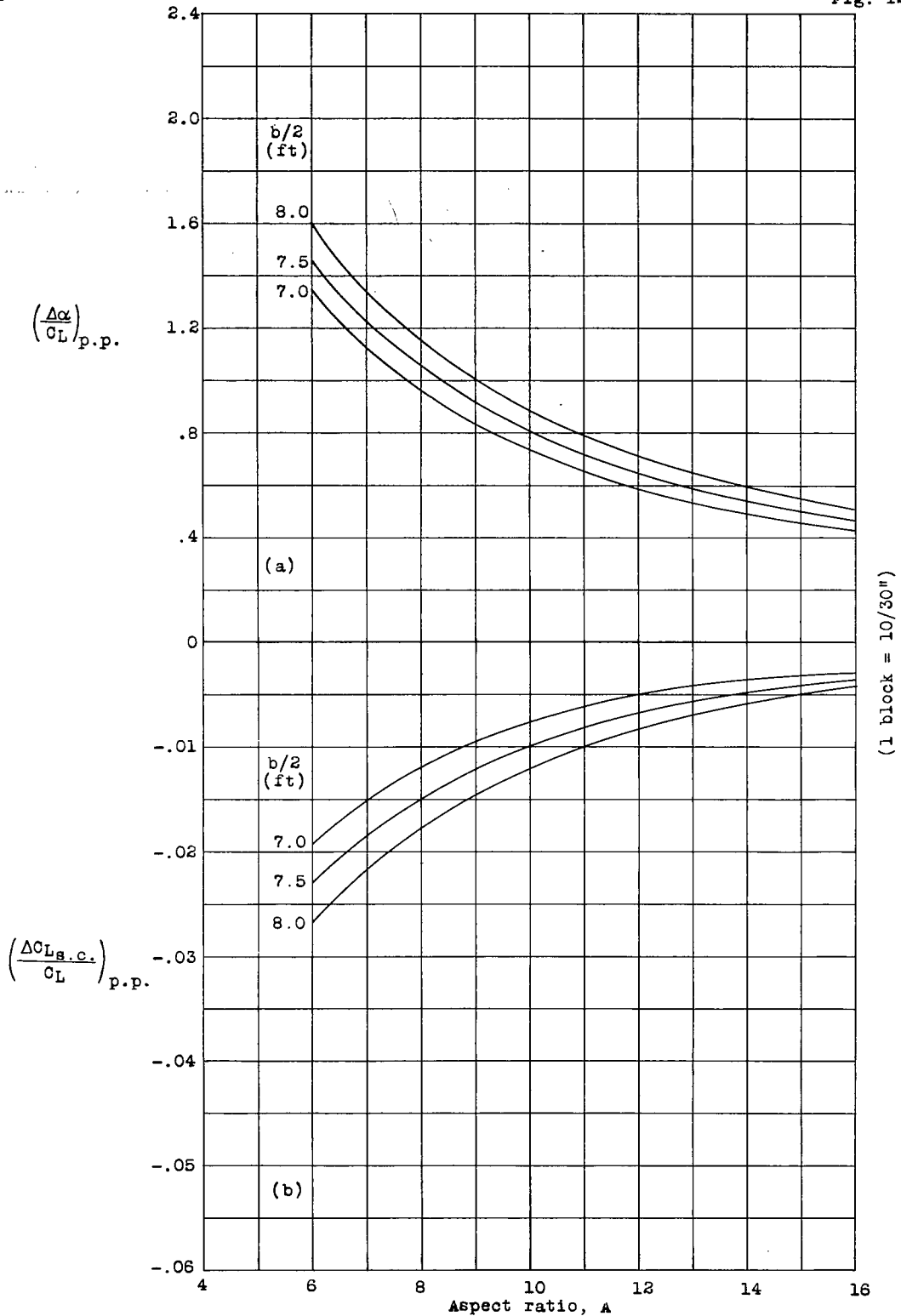


Figure 12 (a to d).- Charts for determining the corrections to the angle of attack, the lift, drag, and yawing-moment coefficients of symmetrically loaded reflection-plane models mounted in 7-by 10-foot closed rectangular wind tunnels.

NACA

Fig. 12c,d

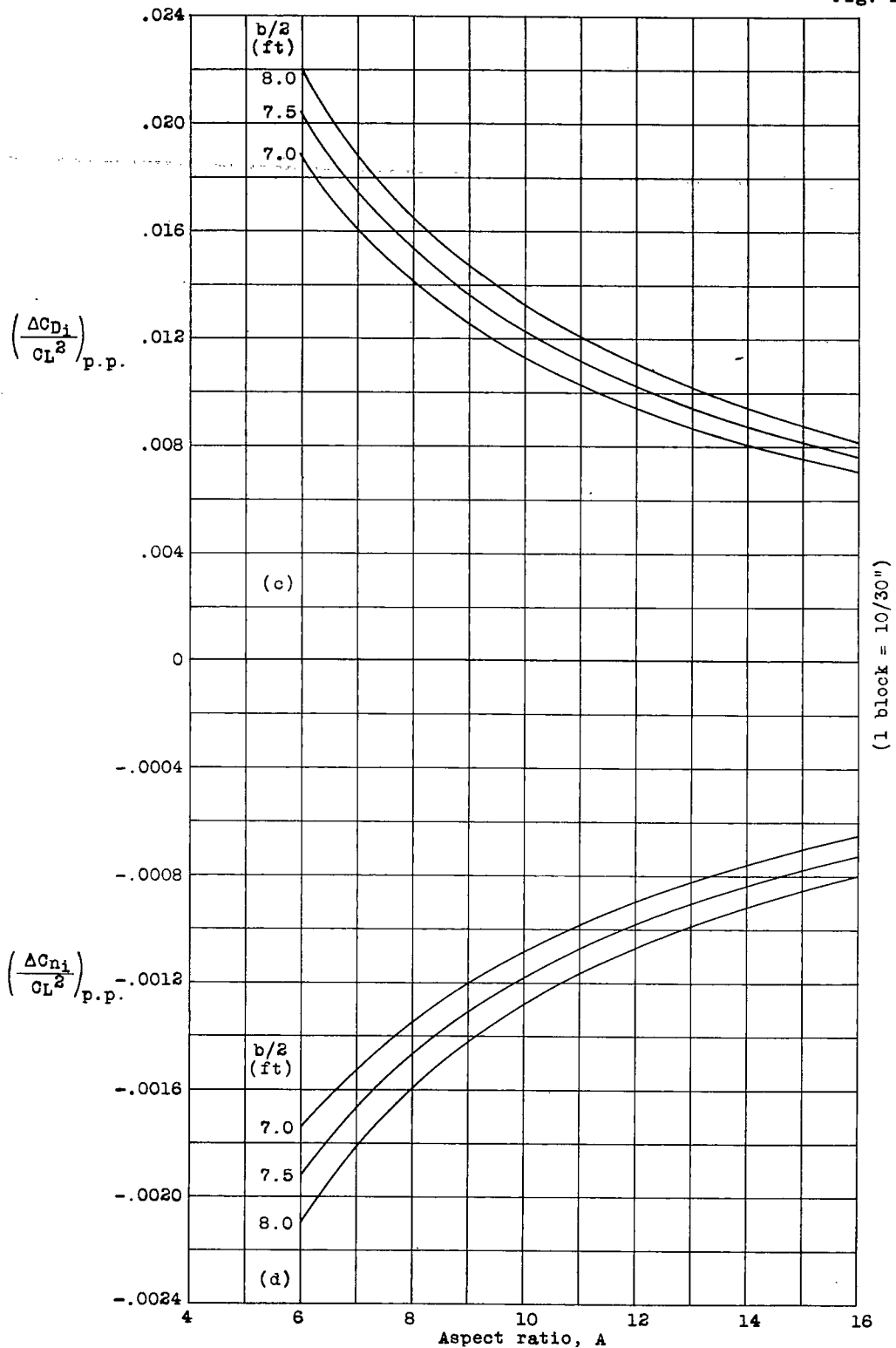


Figure 12.- (Concluded)

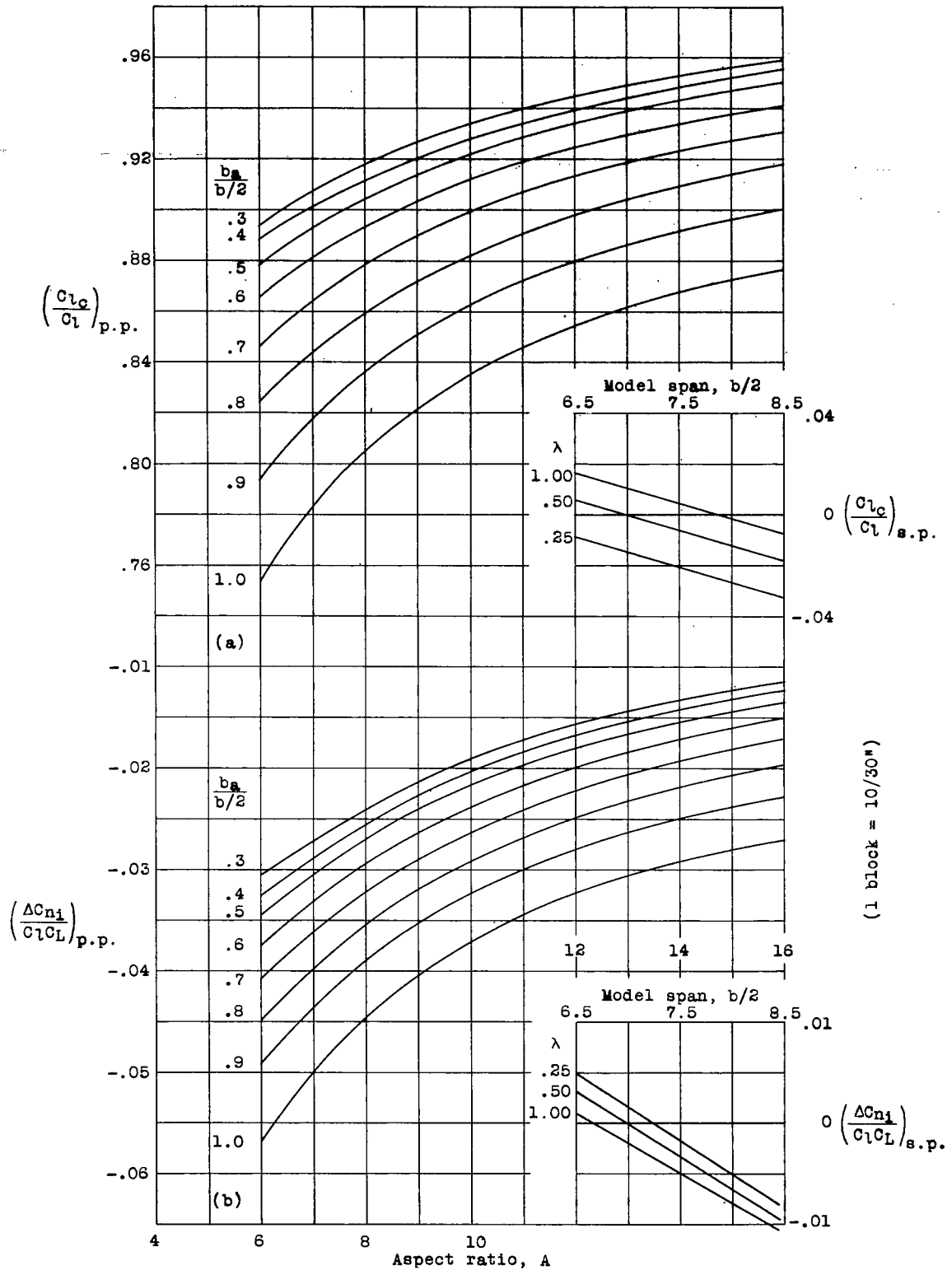


Figure 13.- Charts for determining the corrections to the rolling and yawing-moment coefficients of asymmetrically loaded reflection-plane models mounted in 7-by 10-foot closed rectangular wind tunnels.

NACA

Fig. 14

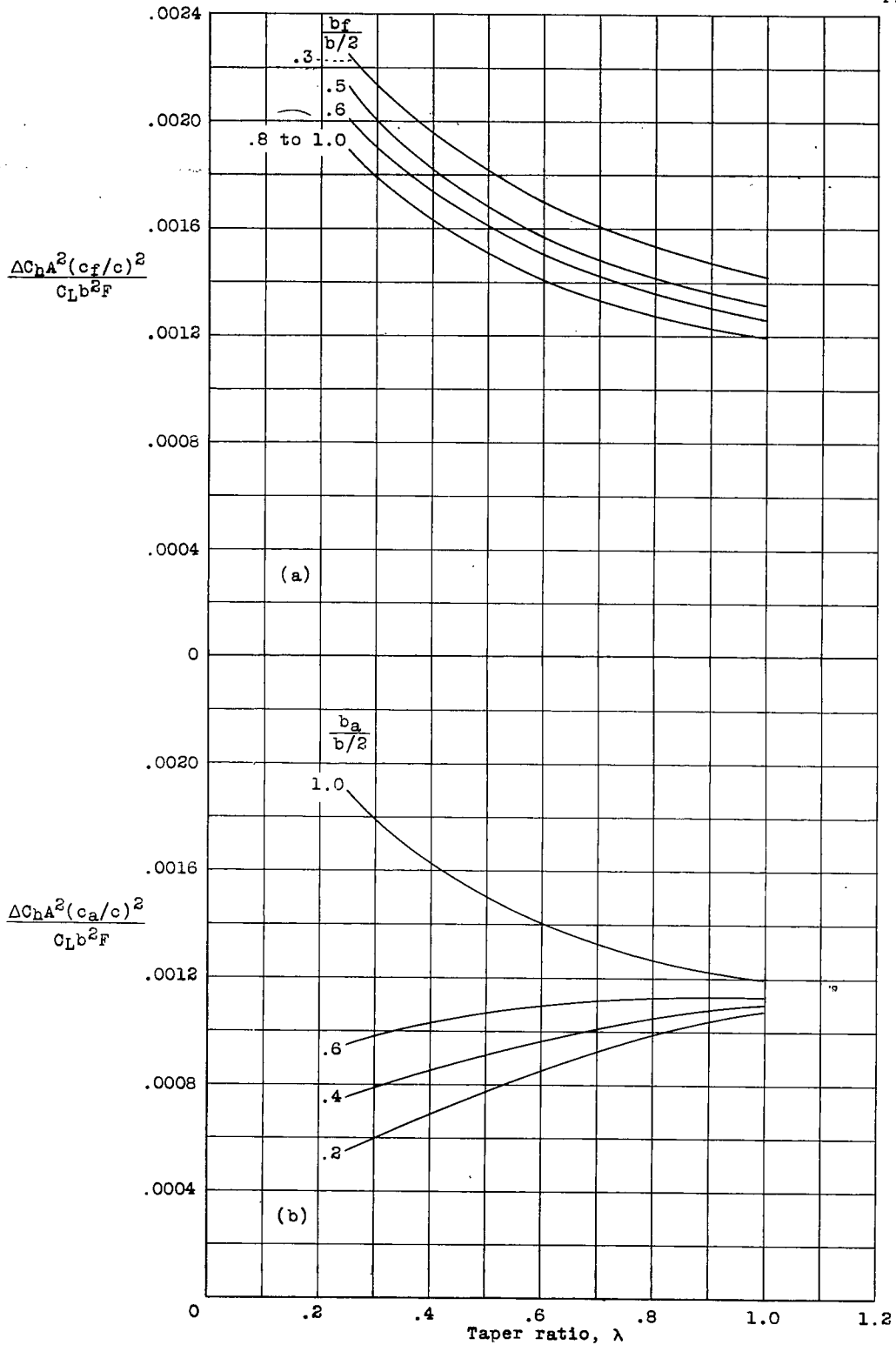


Figure 14.- Charts for determining the corrections, due to streamline curvature, to the flap and aileron hinge-moment coefficients of reflection-plane models mounted in 7-by 10-foot closed rectangular wind tunnels.

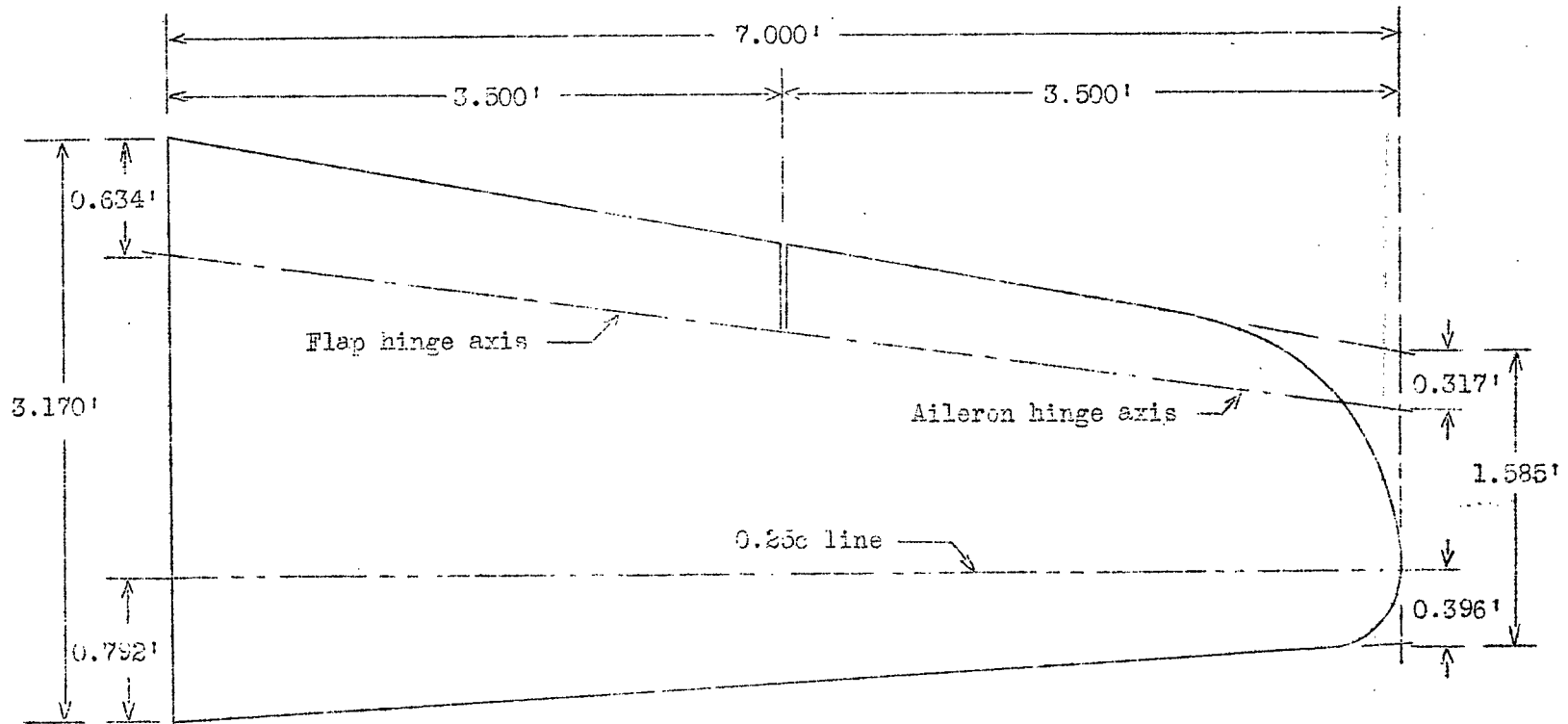


Figure 15.- Plan form of the semispan wing model used for the illustrative example. $A = 8$; $\lambda = 0.5$; $c_f/c = 0.2$; $c_a/c = 0.2$.

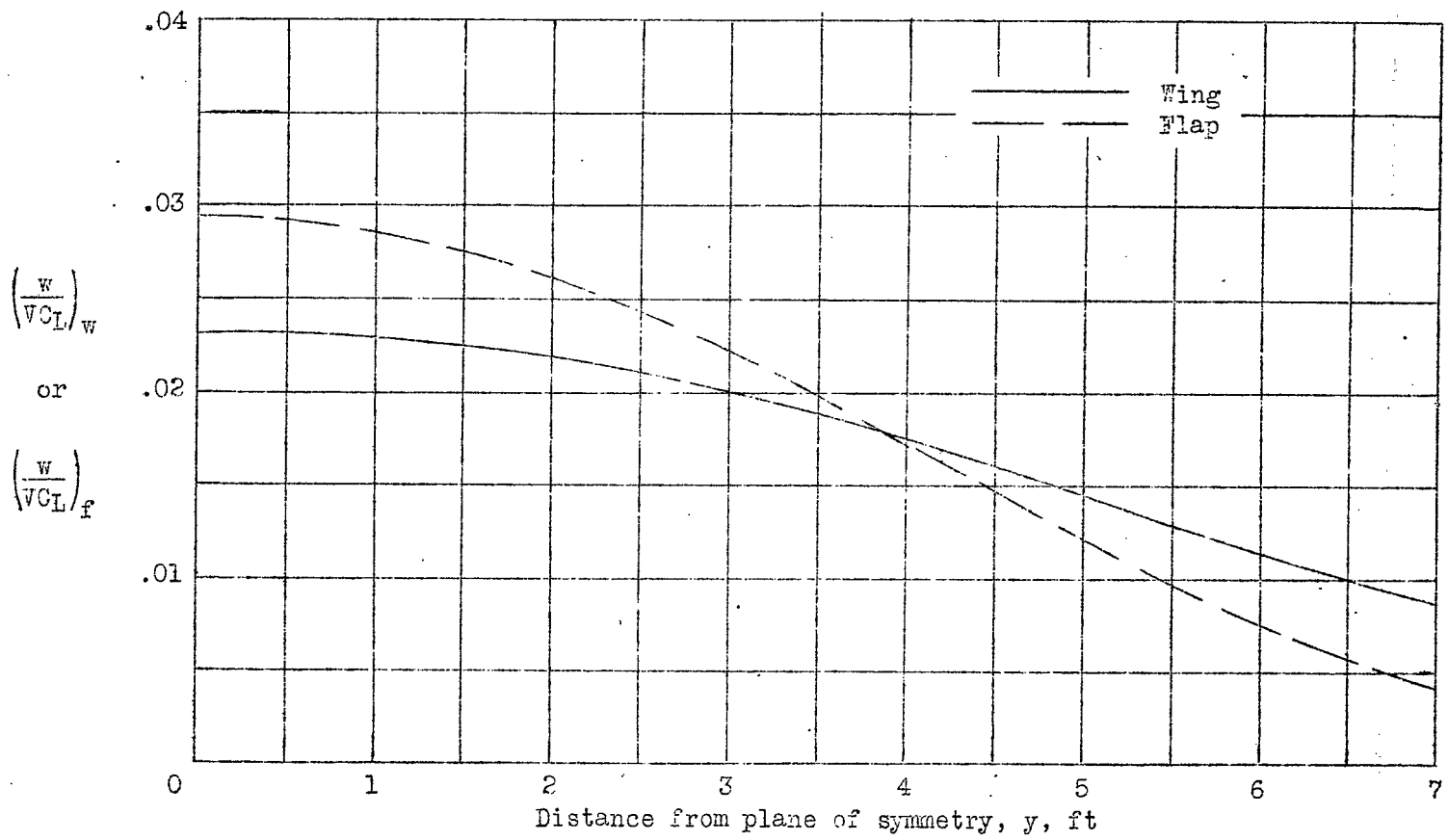


Figure 16.- Variation of the boundary-induced upwash angle, due to the wing and due to the flap, along the semispan of the model used for the illustrative example.

NACA

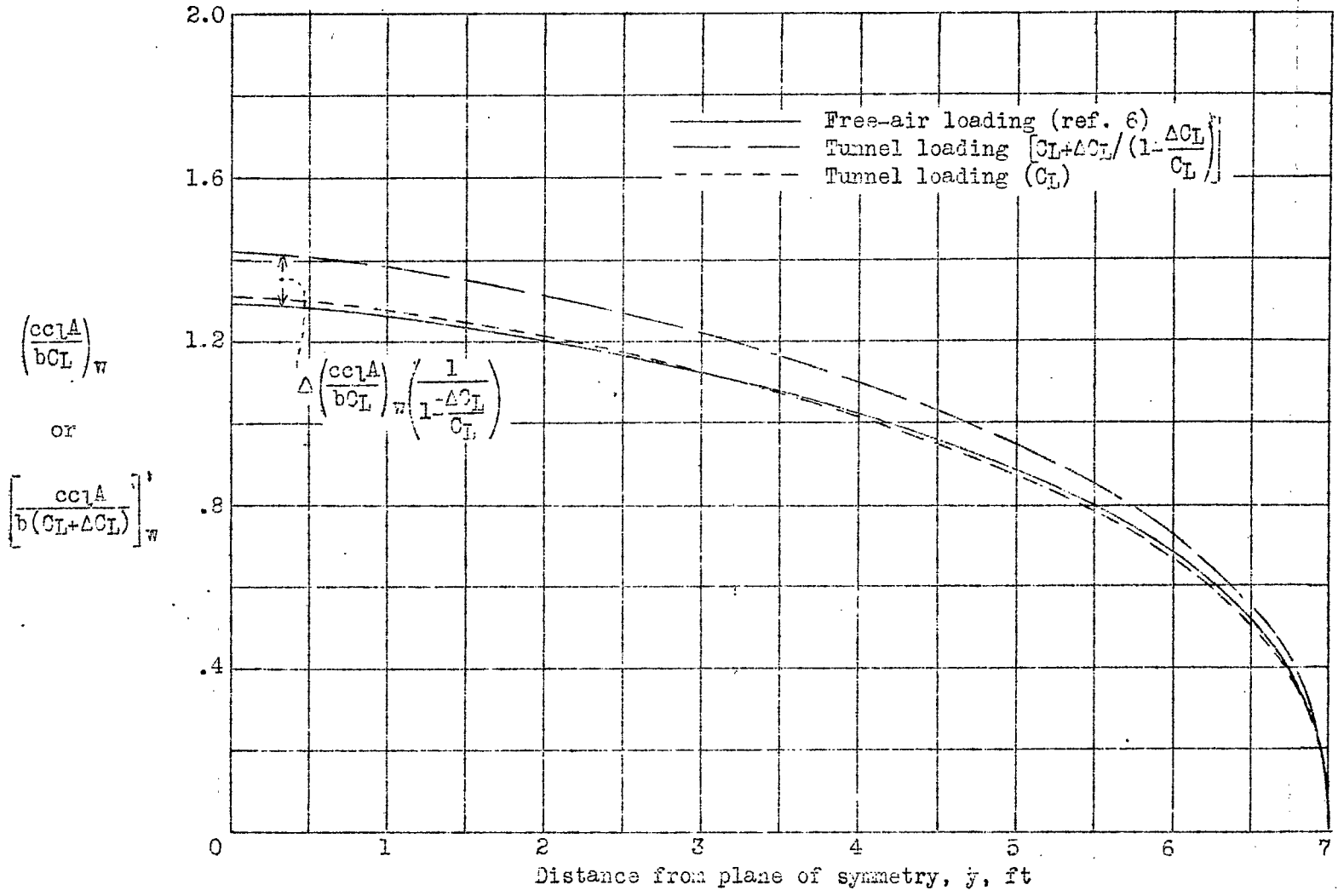


Figure 17.- Free-air and tunnel span load distributions for the wing used for the illustrative example.

FIG. 17

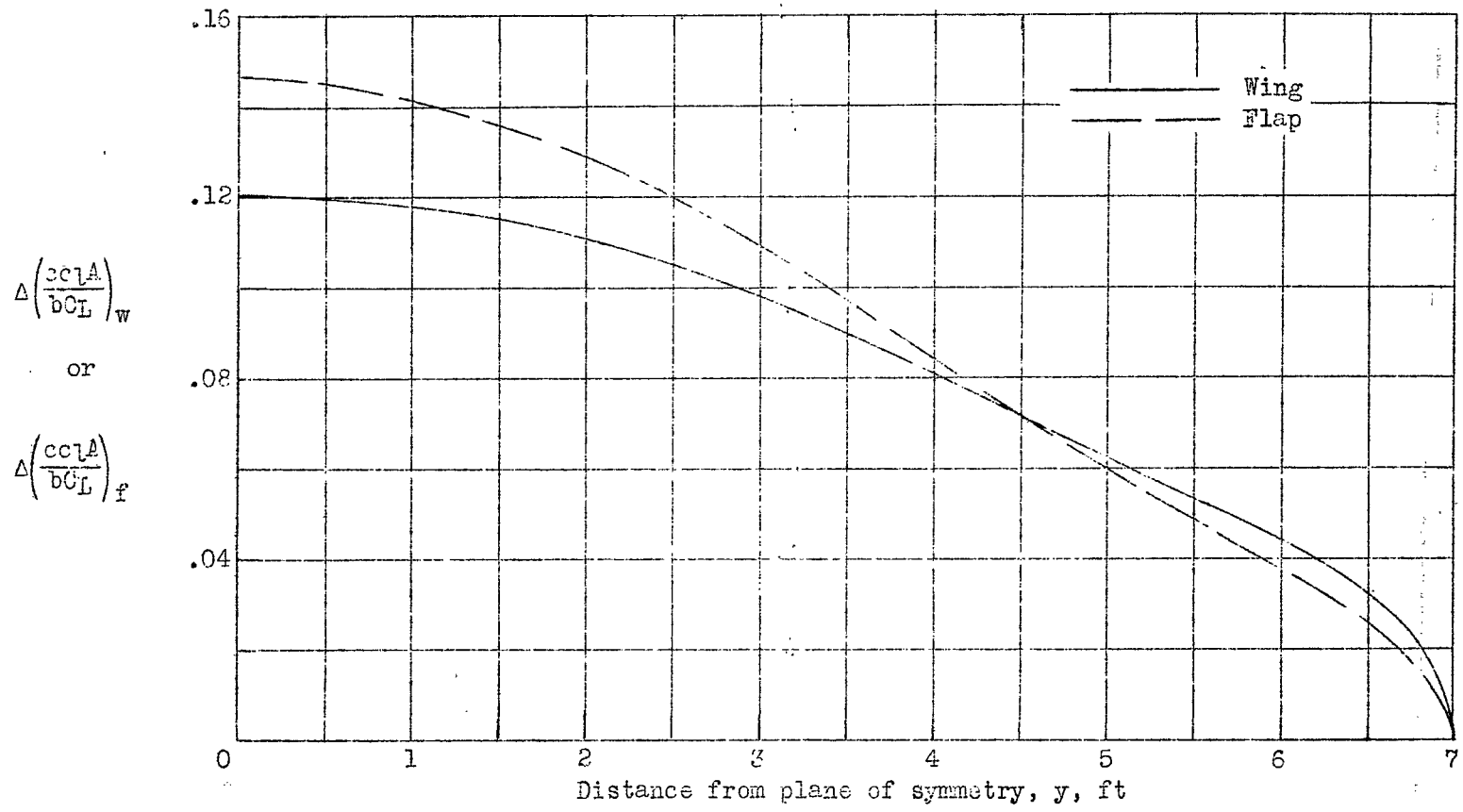


Figure 18.- Variation of the boundary-induced increment of load, due to the wing and due to the flap, along the semispan of the model used for the illustrative example.

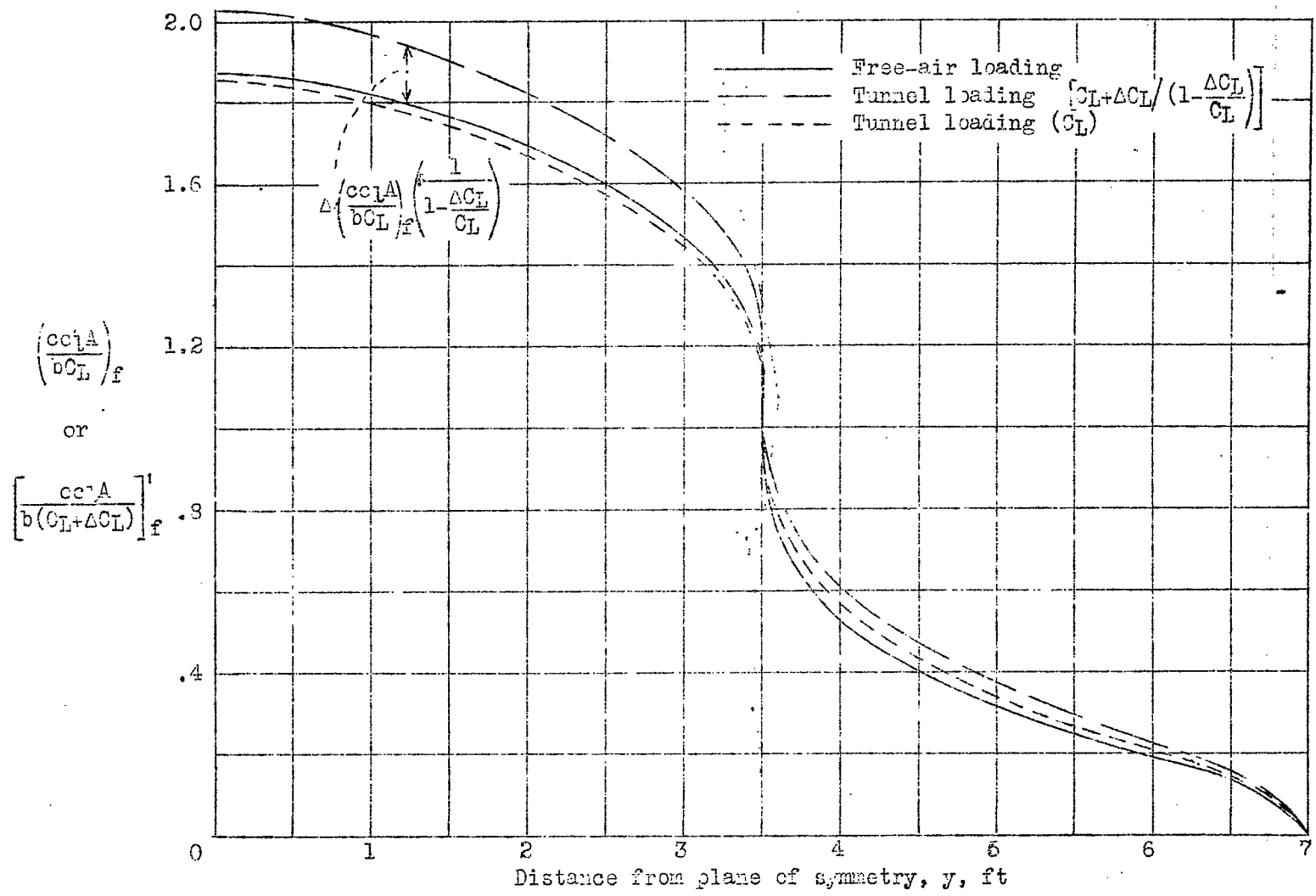


Figure 19.- Free-air and tunnel span load distributions for the flap of the model used for the illustrative example.

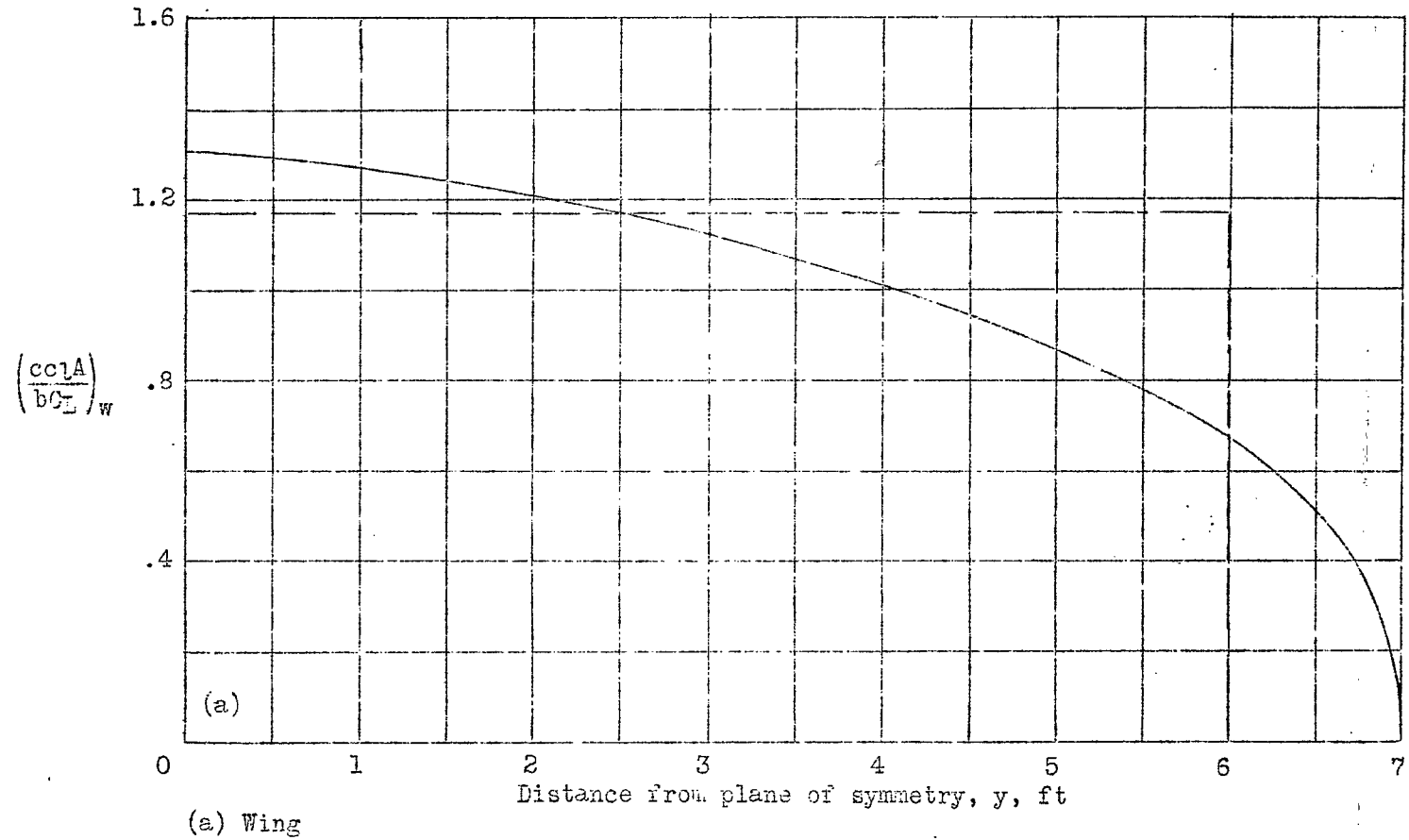


Figure 20a,b.- One-step approximation to the wing load curve and two-step approximation to the flap load curve used for computation of corrections due to streamline curvature for the illustrative example.

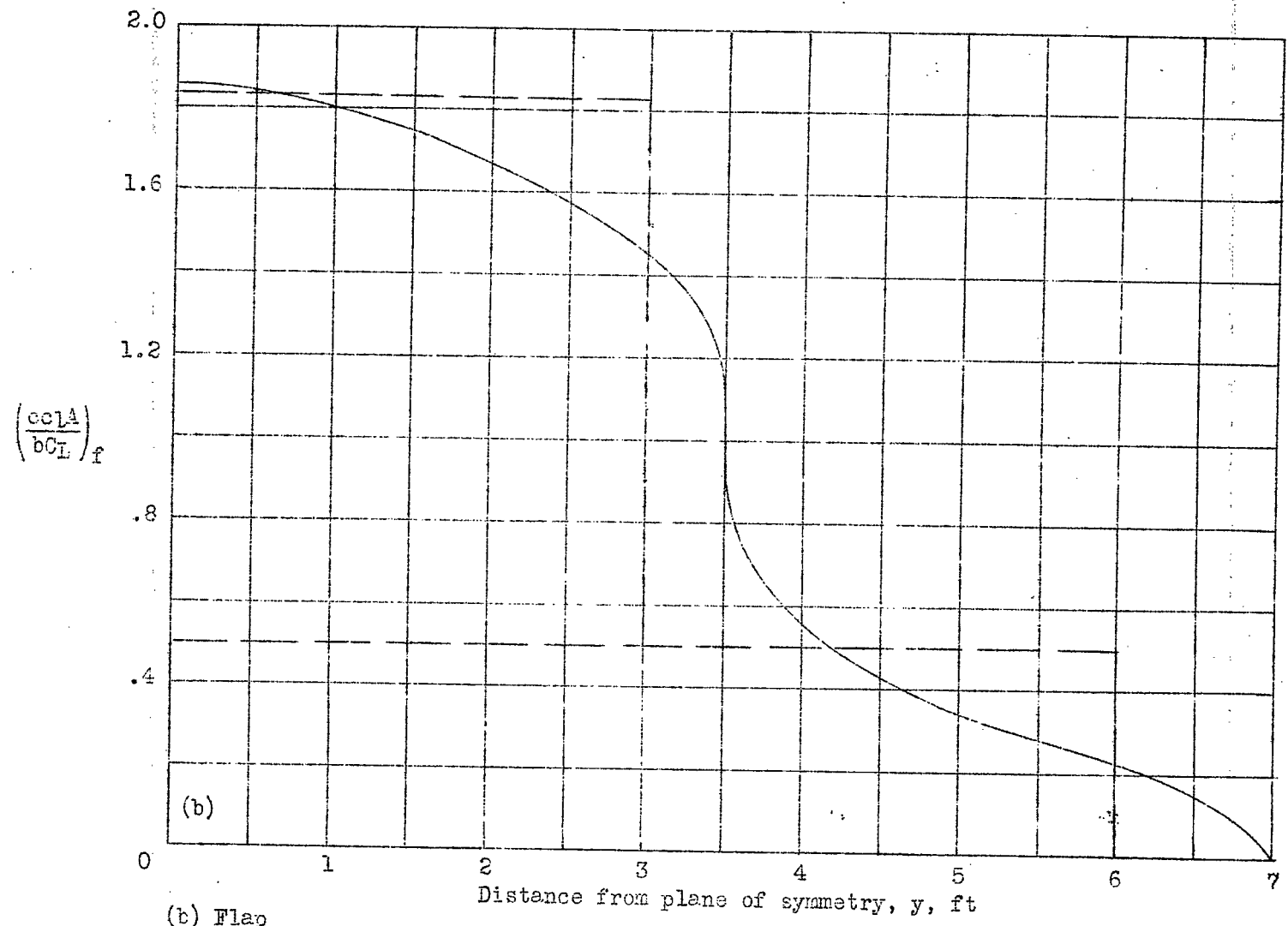


Figure 20.- (Concluded)

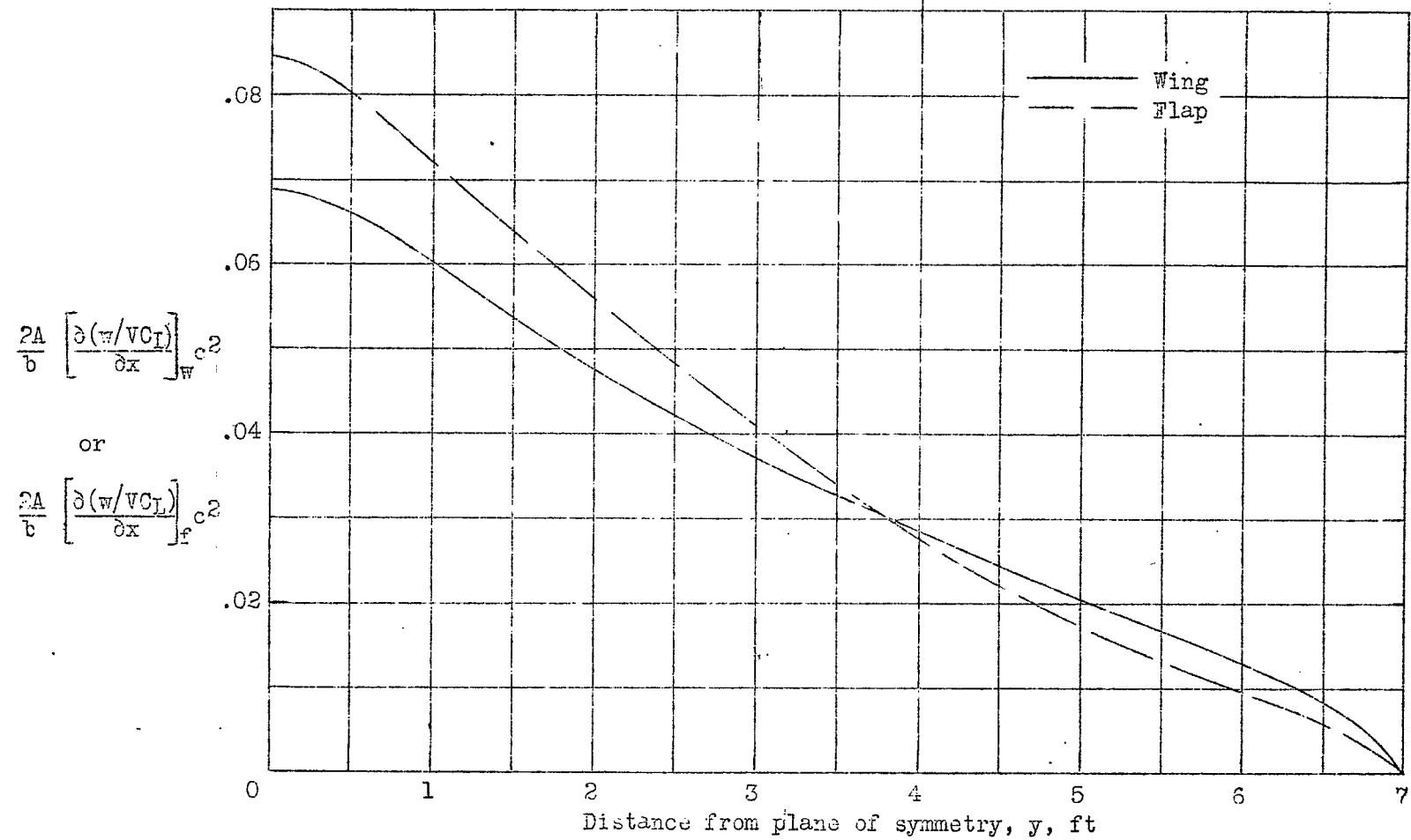


Figure 21.- Variation of $\frac{2A}{b} \left[\frac{\partial(w/V_{CL})}{\partial x} \right]_w c^2$ and $\frac{2A}{b} \left[\frac{\partial(w/V_{CL})}{\partial x} \right]_f c^2$ along the semispan of the model used for the illustrative example.

NACA

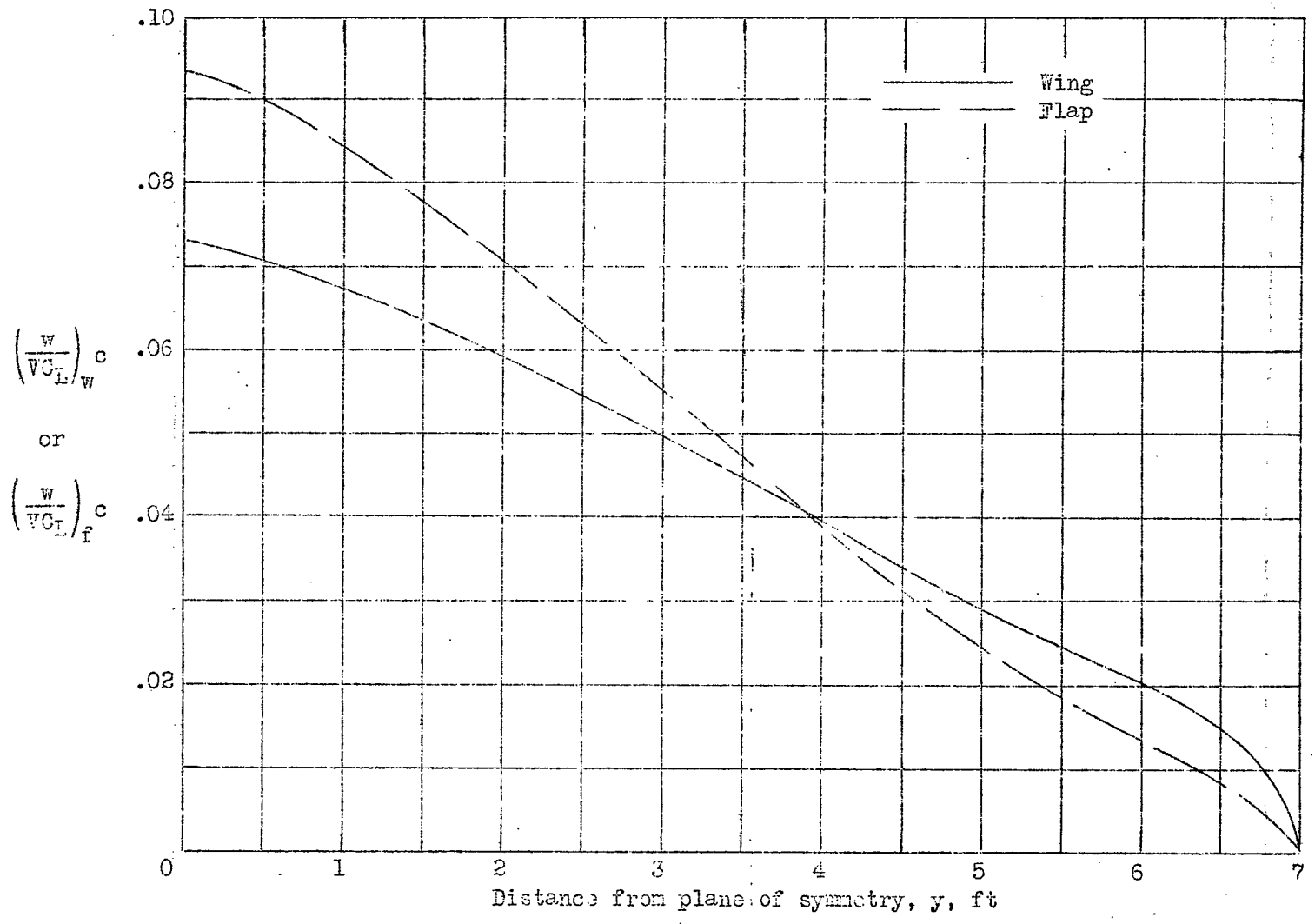


Figure 22.- Variation of $(w/VC_L)c$ along the semispan of the model used for the illustrative example.

FIG. 22

NACA

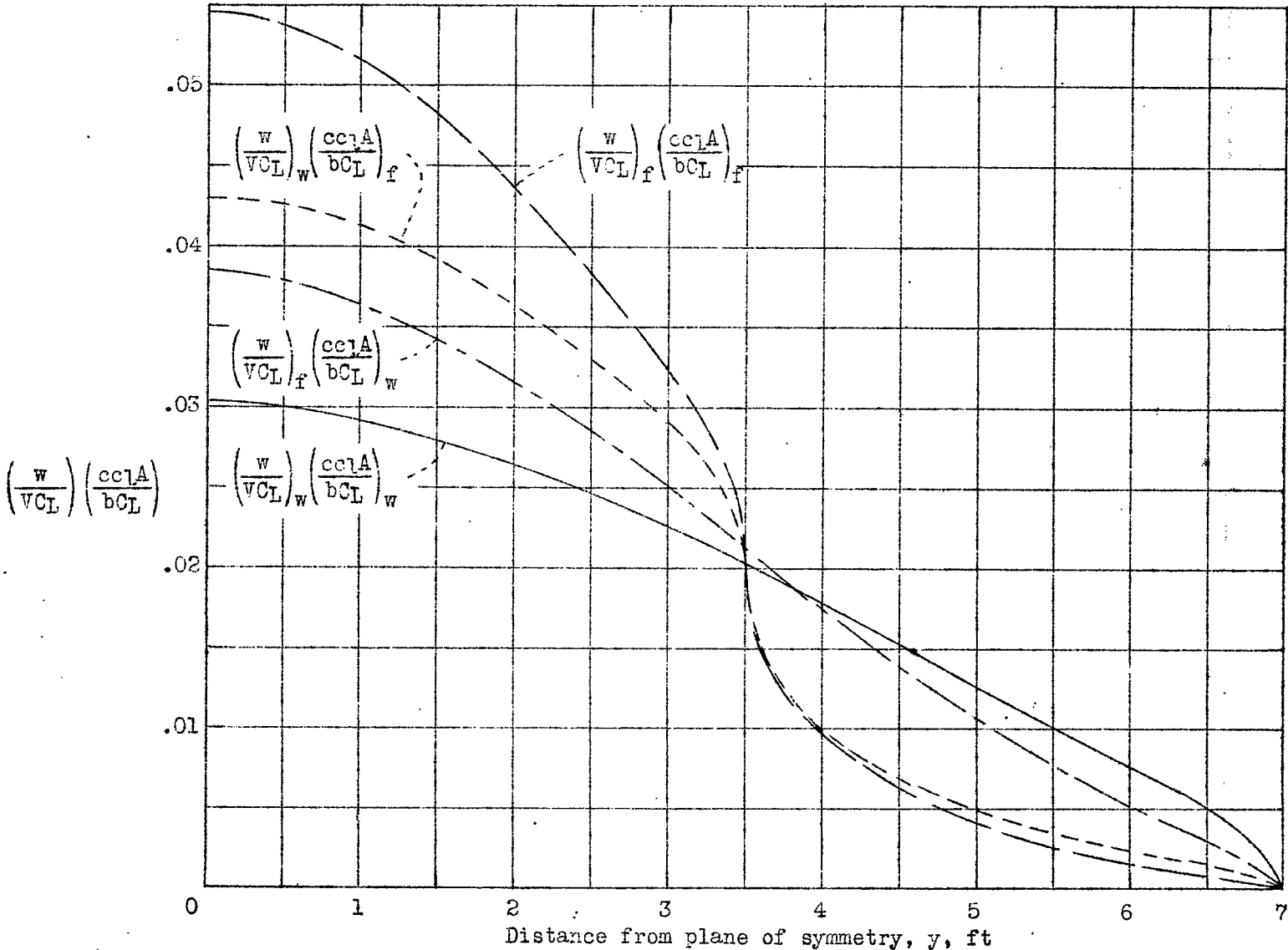


Fig. 23

Figure 23.- Variation of the parameters used to compute the induced-drag and yawing-moment corrections, for symmetrical loading, along the semispan of the model used for the illustrative example.

NACA

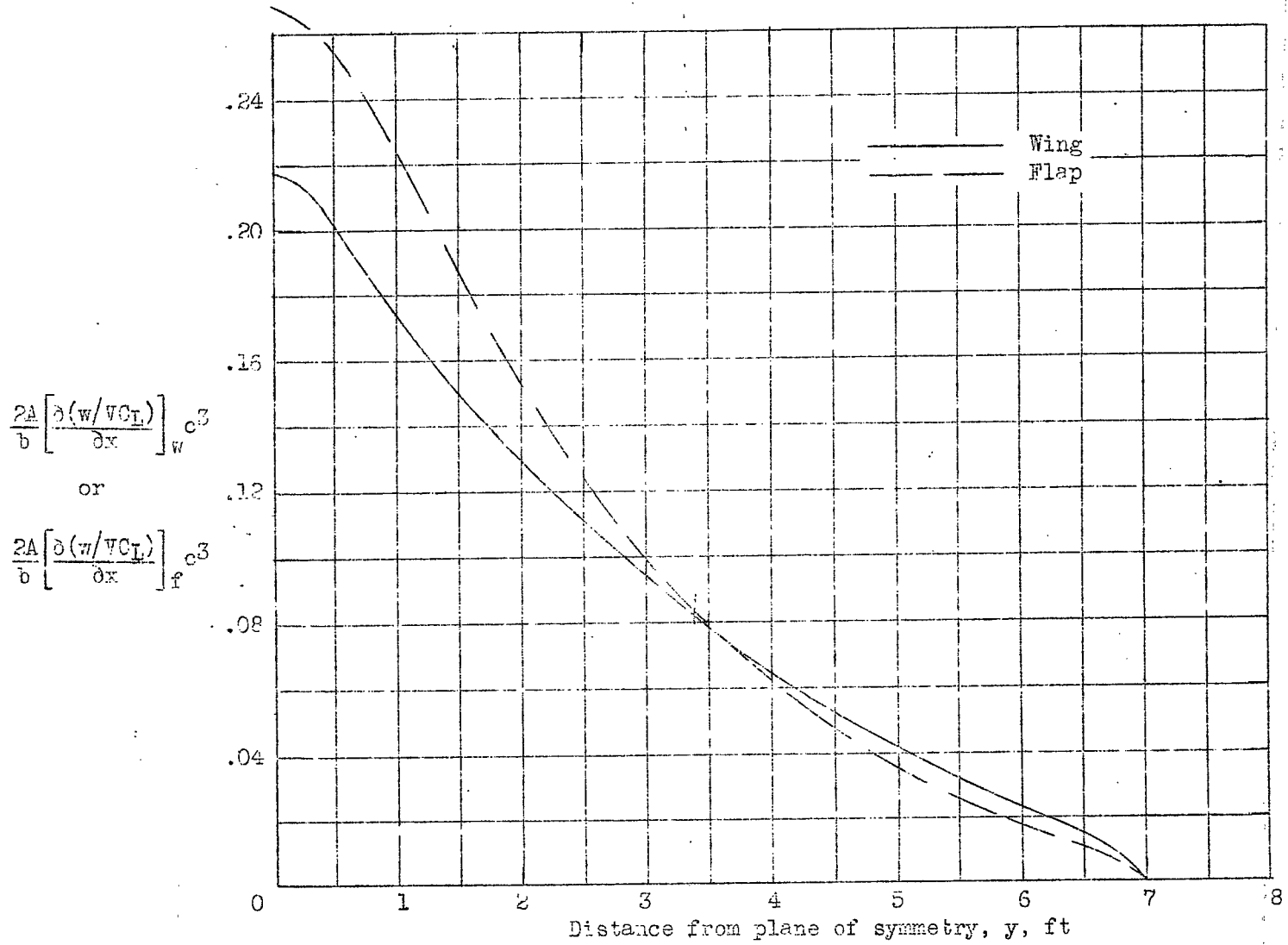


Figure 24.- Variation of $\frac{2A}{b} \left[\frac{\partial(w/VCL)}{\partial x} \right]_w c^3$ and $\frac{2A}{b} \left[\frac{\partial(\pi/VCL)}{\partial x} \right]_f c^3$ along the semispan of the model used for the illustrative example.

Fig. 24

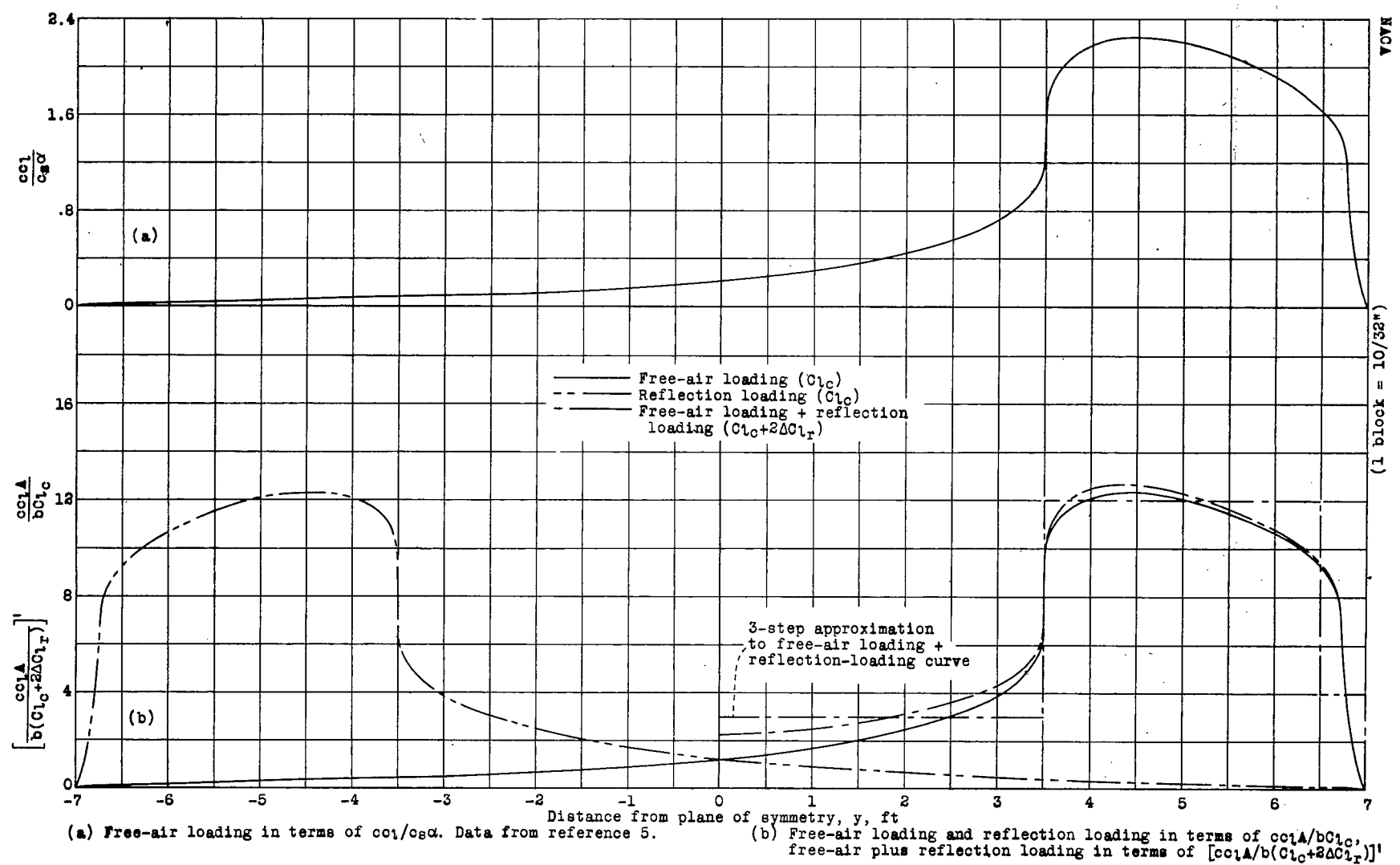
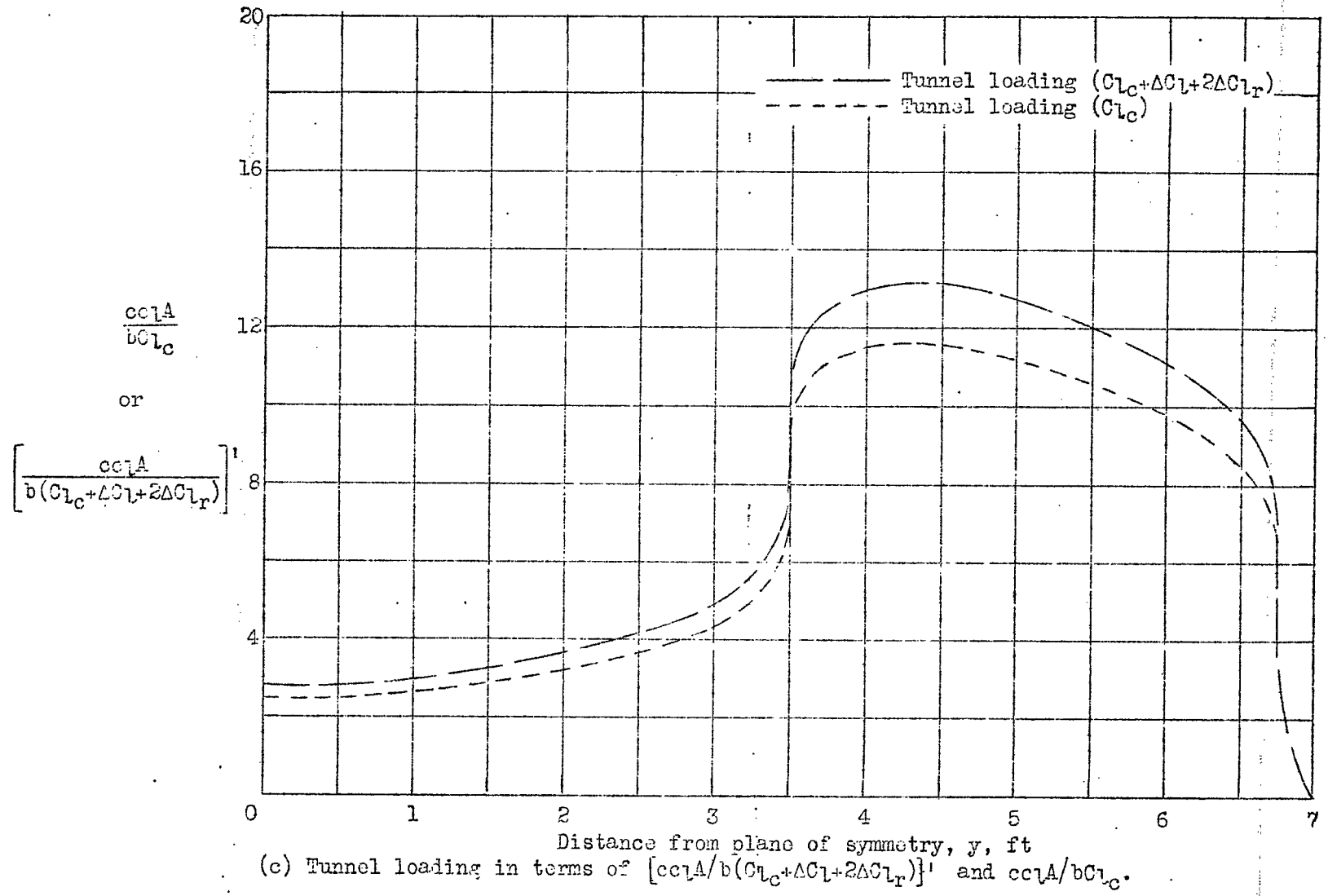


Figure 25.- Development of the tunnel span load distribution due to the deflection of the aileron of the model used for the illustrative example.

NACA



(c) Tunnel loading in terms of $\left[\frac{cc_1A}{b(C_{l_c} + \Delta C_{l_1} + 2\Delta C_{l_r})} \right]^1$ and $\frac{cc_1A}{bC_{l_c}}$.

Figure 25.- (Concluded)

Fig. 25c

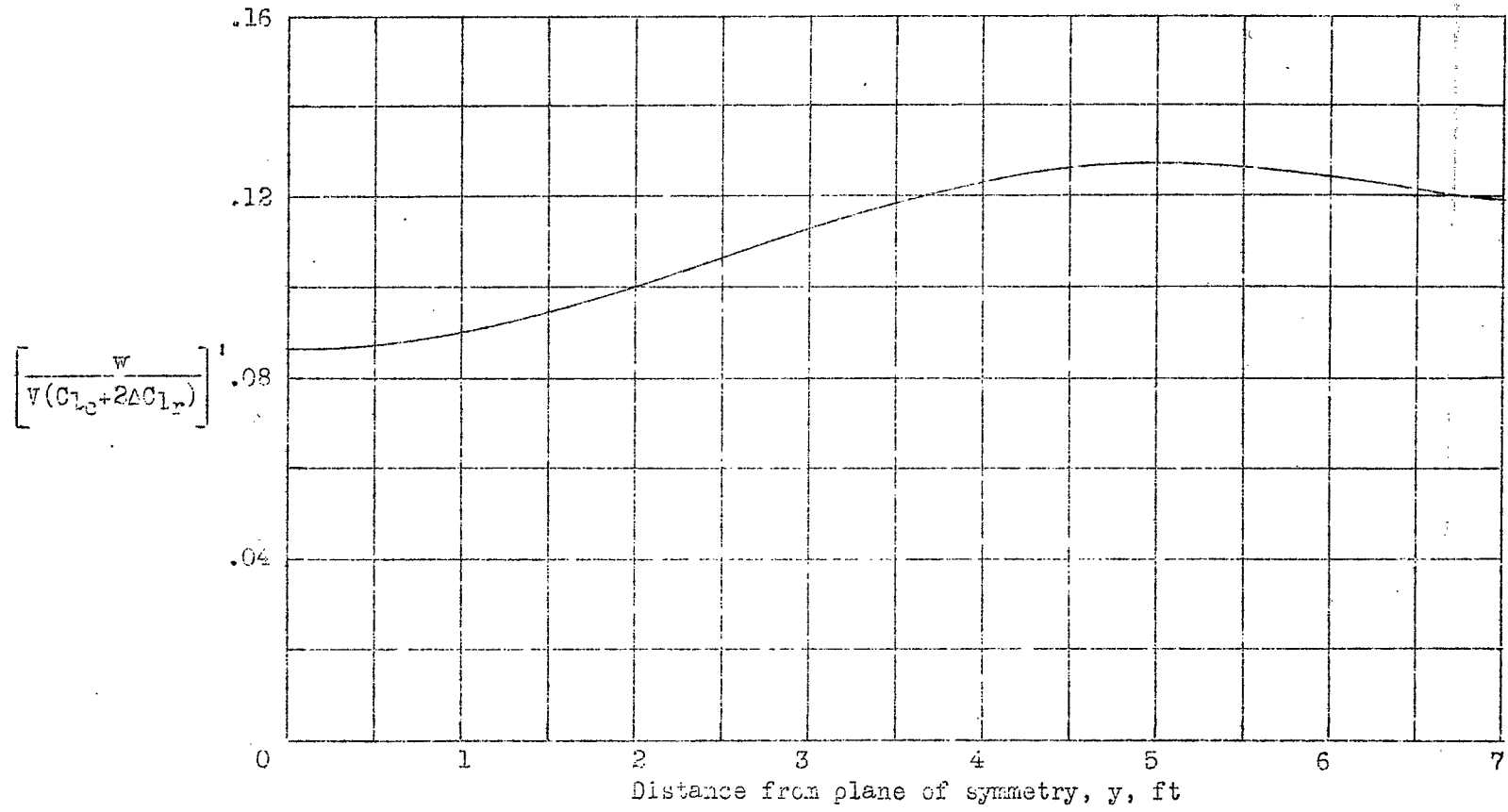


Figure 26.- Variation of the boundary-induced upwash angle, due to aileron deflection along the semispan of the model used for the illustrative example.

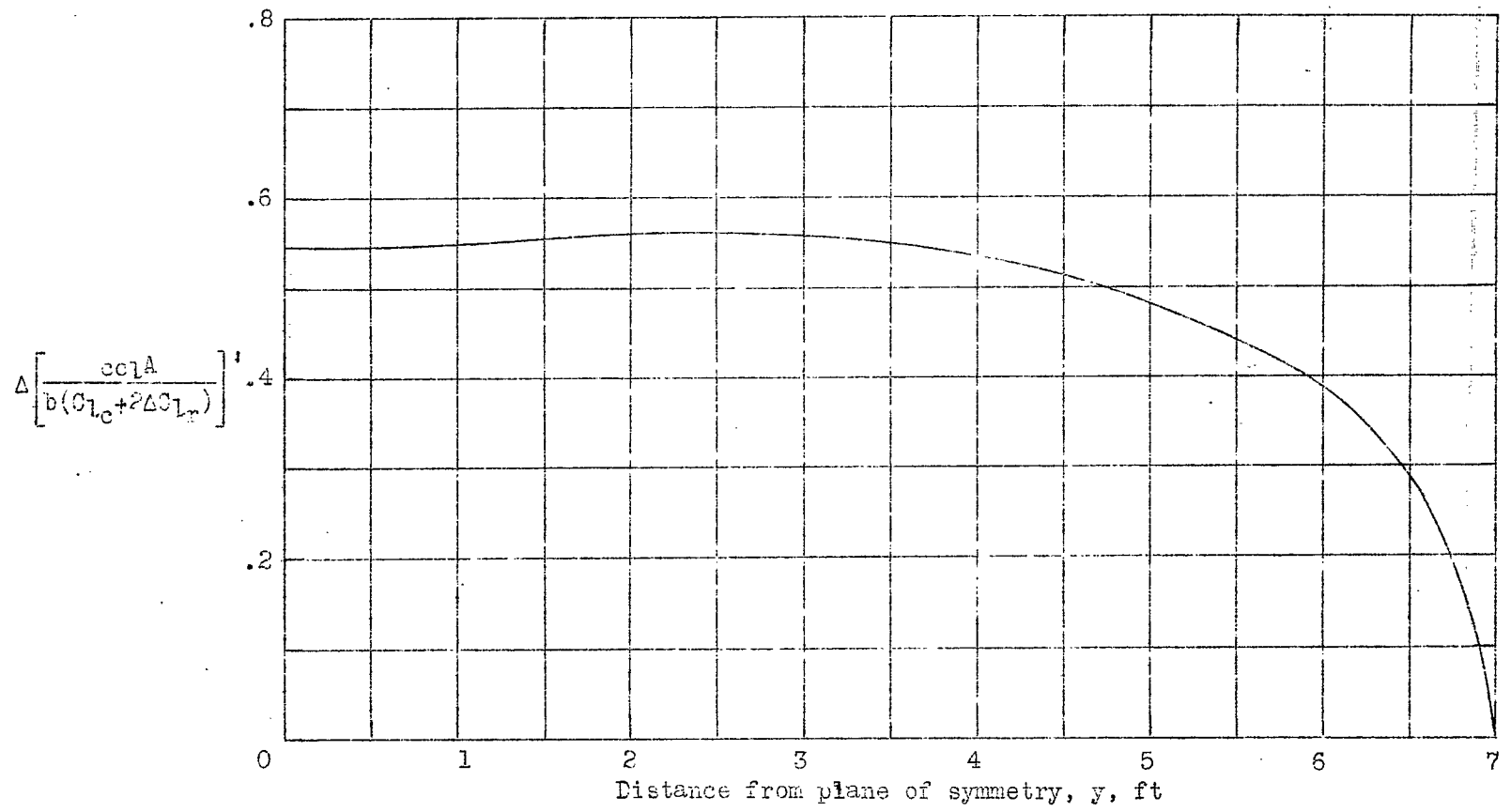


Figure 27.- Variation of the boundary-induced increment of load, due to aileron deflection, along the semispan of the model used for the illustrative example.

MACA

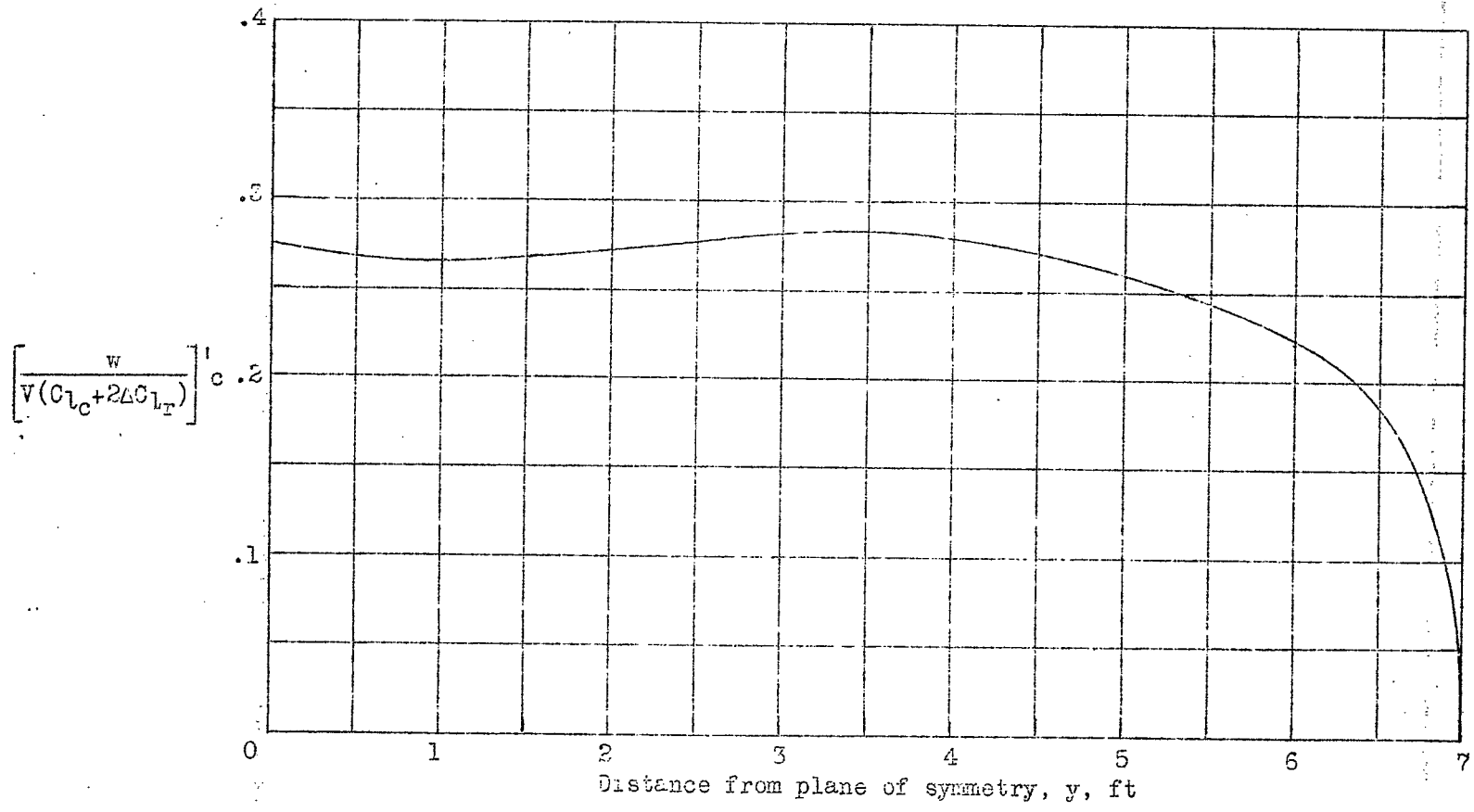


Figure 28.- Variation of $\left[\frac{w}{V(Cl_c + 2\Delta Cl_r)} \right]^1 c$ along the semispan of the model used for the illustrative example.

Fig. 28

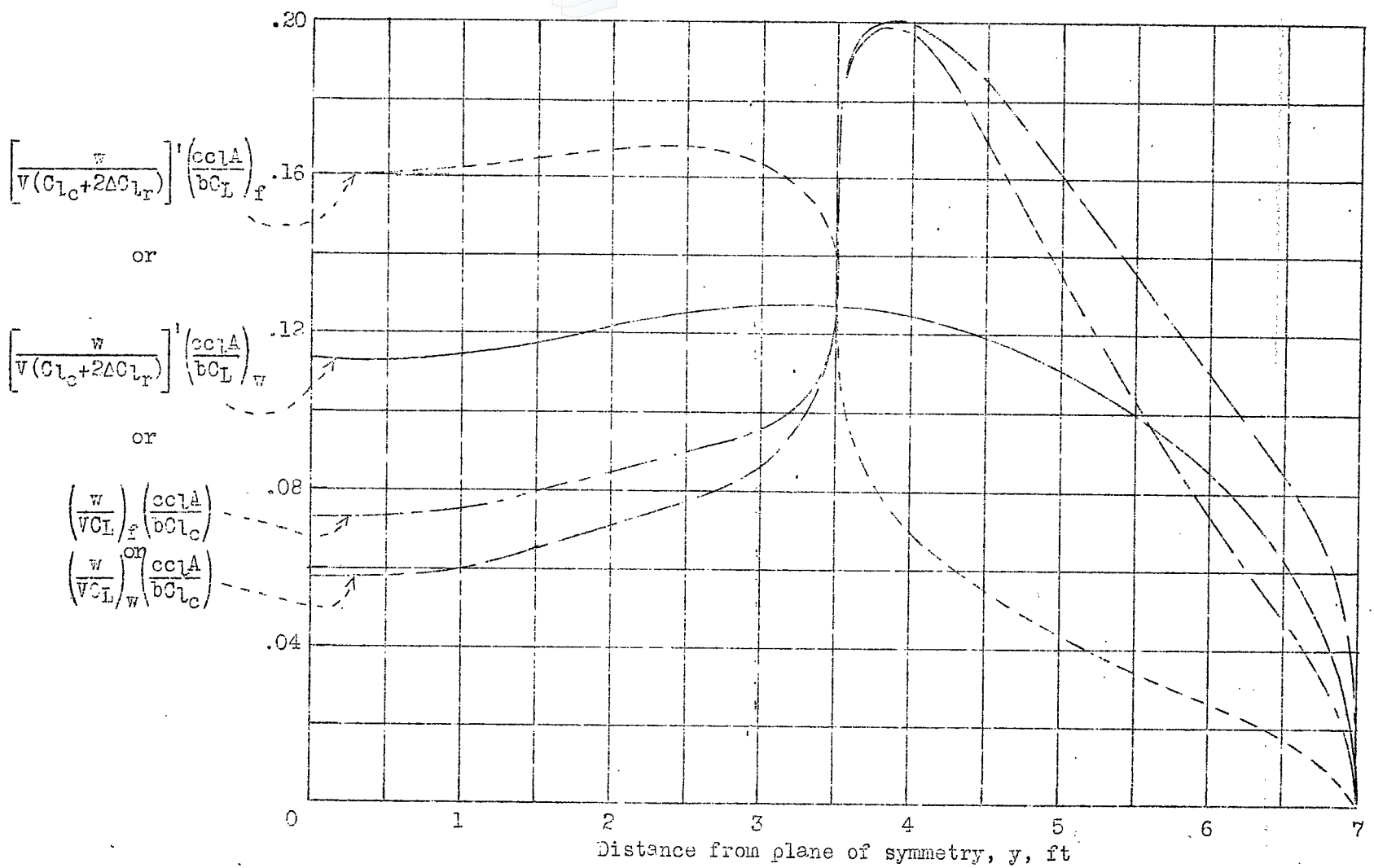


Figure 29.— Variation of the parameters used to determine the induced-yawing-moment correction due to aileron deflection along the semispan of the model used for the illustrative example.

THIS DOCUMENT PROVIDED BY THE ABBOTT AEROSPACE



TECHNICAL LIBRARY

NASA Technical Library

WWW.NASA-TECHNICAL-LIBRARY.NASA.GOV



3 1176 01439 3707